Ni-WC/Al$_2$O$_3$ and Ni-WC/MgWO$_4$/MgAl$_2$O$_4$ catalysts for resource recovery via pyrolysis combined with the dry reforming of plastics (PCDR)

Izabela Wysocka [a,*], Jakub Karczewski [b], Michał Maciejewski [b], Barbara Kościelska [b], Adam Kubiak [c], Andrzej Rogala [a], Jacek Gębicki [a]

[a] Gdańsk University of Technology, Faculty of Chemistry, Department of Process Engineering and Chemical Technology, Narutowicza 11/12 St., 80-233 Gdańsk, Poland
[b] Gdańsk University of Technology, Faculty of Applied Physics and Mathematics, Institute of Nanotechnology and Materials Engineering, Narutowicza 11/12 St., 80-233 Gdańsk, Poland
[c] Adam Mickiewicz University, Faculty of Chemistry, Uniwersytetu Poznanskiego 8, PL-61614 Poznań, Poland

ARTICLE INFO

ABSTRACT

Plastic waste (PW) is currently one of an environmental threat. Despite the increasing share of recycled plastics, their disposal remains high. Therefore, there is a high demand for new PW management systems. Among them, pyrolysis combined with dry reforming (PCDR) is an advantageous solution because it allows for resource recovery in the form of gas and liquid fuels, with simultaneous utilization of CO$_2$. To date, catalysts based on Ni, Co, and noble metals supported on metal oxides have been examined. However, these catalysts suffer from quick deactivation due to coking and sintering. Therefore, testing other materials for PCDR is of particular importance. In this regard, Ni-WC/Al$_2$O$_3$ and Ni-WC/MgWO$_4$/MgAl$_2$O$_4$ were investigated as potential PCDR catalysts. The catalysts were characterized by BET, BJH, XRD, CO$_2$-TPD, H$_2$-TPR, SEM, TEM, TG and DTG. The catalytic activity was evaluated in a two-step PCDR process using low-density polyethylene (LDPE), polystyrene (PS), polyethylene terephthalate (PET), and simulated waste plastic (SWP). The structure of the polymer strongly determines the yields of gas, liquid, and solid products. The highest yield of synthetic gas generation was observed for Ni-WC/MgWO$_4$/MgAl$_2$O$_4$ and was 48.20 ± 2.41 mmol/g$_p$. Different origins of the structural changes including oxidation or coking were observed for different plastics. PCDR of PET led mainly to oxidation, LDPE to the coking deposition. Catalysts after the process with PS were characterized by preservation of crystalline structure. The results indicate a high potential of carbide catalysts in the recovery of gaseous and liquid raw materials.

1. Introduction

The depletion of fossil fuels and the global energy crisis have forced the search for new alternative energy sources and substrates for the chemical industry. Plastic materials may be used once or multiple times, depending on the purpose and quality of production. However, a significant share of plastics made out of fossil fuels is disposed of in landfills, especially when their recycling is difficult to process due to even minor damage, low quality, or legal standards. For example, disposable gloves can only be used once for medical purposes. This problem was particularly evident during the Covid-19 pandemic when the demand for disposable packaging and personal protective equipment was particularly high [1,2]. Therefore, the problem of plastic waste in the environment is more visible than usual. Despite the threat to aquatic and terrestrial organisms, the increasing abundance of plastics in the environment may retard efforts to fulfil sustainable development goals

(SDGs), especially those connected with climate action, life below water, and land. The landfilling of plastics can also lead to their fragmentation and atmospheric aging, and consequently to the environment in the form of microplastics. As a result of atmospheric aging, structural changes can also occur leading to leaching and release of hazardous compounds into the environment [3,4].

Therefore, the search for new methods for plastic waste management has been the subject of many extensive studies [3,5–9]. Municipal waste, including plastic waste that cannot be recycled and reused to restore plastic materials, may be used for energy purposes via incineration. Another method for managing waste plastics is to use them in syngas production. Synthetic gas is one of the most important primary substrates in the chemical industry. Currently, synthetic gas is mainly produced by steam reforming, gasification, or pyrolysis. The method chosen for syngas generation is determined by the required hydrogen-to-carbon monoxide ratio in the outlet stream. Polymeric materials such as plastics may be an alternative feedstock for synthetic gas production [10–13]. The pyrolysis of plastics both catalytic and uncatalyzed leads to a high content of short-chain gas hydrocarbon and liquid fractions. To enlarge and enrich the syngas in H_2 and CO after pyrolysis step a combining with the reforming units has been proposed [14–19]. Depending on the intended use, the parameters of the outlet stream, including the syngas composition, can be manipulated using appropriate reforming agents: steam and/or carbon dioxide. For applications that require hydrogen-rich syngas steam reforming is used, whereas dry reforming is applied to processes that require carbon-monoxide-rich syngas [18,20–24]:

However, dry reforming methods, mainly dry methane reforming (DRM), are still industrially immature owing to fast catalyst deactivation. The deactivation of catalysts proceeds through the coking, fouling, poisoning, or sintering of metal active particles, leaching of particular elements, or changes in acid-base properties [25–27]. Currently, the most widely used catalysts are based on Ni or Co particles supported on metal oxides. The use of nickel catalysts is economically justified because of their relatively low price and high activity, which are comparable to those of noble metals. Therefore, worldwide research is directed towards the modification of nickel catalysts to improve their properties. The methods for improving catalytic activity and stability include promoting with alkali, D-block and lanthanides elements such as cerium [28], calcium, magnesium, lanthanum, potassium, gadolinium, scandium, manganese and iron [21,24,29,30]. The modification with promoters such as La or Ga may lead to increased basicity, enhanced active metal-support interactions, generation of additional oxygen vacancies, stabilization of metal active phase suppressed carbon deposition [30,31]. Reports in the field of pyrolysis combined with a reforming process, both steam and dry, in the overwhelming majority regard Ni, Co, or noble metal catalysts supported on metal oxides, zeolites, or activated carbon [11,21,24,28,29,32–37]. Recently, increased attention has been paid to carbon-based materials, mainly because of the possibility of their synthesis using renewable or waste materials [38–41].

Among carbon materials, transition metal carbides (TMCs) have attracted considerable interest because of their high thermal stability and catalytic activity. During the dry reforming process, they exhibit high activity and resistance to coking resulting from carburization-oxidation cycles [33,42,43]. During the oxidation CO_2 is reduced to CO, whereas during carburization, carbon atoms from methane cracking and CO disproportionation are incorporated into the carbide structure. This prevents the formation of carbon deposits on the catalyst surface. However, it should be noted that carbides, such as WC, show stable activity only at relatively high pressures. At atmospheric pressure, deactivation of such catalysts occurs during the CO_2 oxidation process, which is a significant limitation. To overcome the limitations associated with coking and oxidation of nickel and carbide catalysts, respectively, combining these two types of catalysts has been proposed [44]. The presence of Ni or Co may promote the formation of crystalline carbide structures [45–48]. Moreover, metal carbide particles during the DR of

hydrocarbons promote the activation of carbon dioxide molecules by facilitating the formation of oxygen vacancies and retarding coke deposition. Zhang et al. [41] reported that coupling nickel particles with a Co-WC/activated carbon catalyst enhanced the activity and stability in the dry reforming of methane by promoting carbon penetration into the tungsten lattice and changing the oxygen environment of the catalyst. Transition metal carbides may exhibit high stability during biomass reformation. Lalsare et al. [49] reported that Fe-Mo_2C-CNF (CNF stands for carbon nanofibers) is effective, stable catalyst for CH_4-CO_2 assisted biomass reforming. After 15 cycles, the catalytic activity and molybdenum carbide structure were preserved. The Mo_2C remained stable in β-Mo_2C form, whereas iron molecules underwent reaction with under-coordinated carbon and from generated coke. However, there are also reports in the literature on the negative effect of nickel on the catalytic activity of carbides. Kim et al. [50] observed that the deposition of nickel on tungsten carbide particles may promote the formation of surface carbon and severe particle aggregation during the hydrocracking of vacuum residue.

Among the methods for transition metal synthesis, three main methods can be distinguished: high-temperature sintering of particular elements (Mo, W, C, Ti, etc.) [51] or their oxides [52] under inert conditions [53], carburization of metal oxides (WO_3, MoO_3) under reductive and carbon-rich atmospheres (methane/H_2 [54–56], ethane/H_2 [55,57,58]), and carburization of organic-inorganic precursors (e.g., amine-MoOx [59,60], WOx combined with amine [46], corn starch [61], chitin [62], activated carbon or carbon black [63]). The use of the method of producing an organic-inorganic precursor allows for the synthesis of carbide materials under much safer conditions than synthesis in a stream of hydrogen and hydrocarbons. Moreover, the use of renewable (biomass, saccharides) or waste materials as carbon for metal carbide preparation has been gaining increasing attention. Adapting synthesis' methods that allow the use of sustainable substrates may contribute to the development of green catalysts. Recently, Mir et al. [64] reported a novel method for molybdenum carbide Mo_2C synthesis using used pipette tip made as a carbon source. In our previous report, we showed high activity of Ni-WC catalysts obtained using mono and disaccharides as a carbon source [48].

Transition metal carbides have been extensively examined for dry reforming of methane. Literature on the investigation of catalytic activity in the dry reforming of other hydrocarbons then CH_4 is scarce. To our best knowledge, there are no reports on the application of Ni-WC supported on metal oxides in pyrolysis combined with dry reforming (PCDR). The aim of this study was to investigate the catalytic stability, activity, and selectivity of nickel-tungsten carbide catalysts supported on metal oxides during the pyrolysis of plastics (PS, PET, LDPE, or simulated waste) combined with the dry reforming process. The effects of the support and plastic type on the activity and stability were investigated. This study contributes to the development of carbide catalytic materials and their application in the recovery of energy and chemical raw materials using a system of coupled pyrolysis and reforming.

2. Materials and methods

2.1. Materials

Nickel nitrate, 6-hydrate (Pol-Aura, ≥99,5 %), and ammonium metatungstate (AMT, Sigma Aldrich, ≥99,99 %) were used as the nickel and tungsten precursors, respectively. Anhydrous glucose (Pol-Aura, ≥99,5 %) was used as the carbon source for the WC preparation. Magnesium nitrate and/or aluminum nitrate were purchased from Pol-Aura (≥99,5 %) and used as precursors for the preparation of $MgAl_2O_4$ spinel and Al_2O_3. Ammonia water (25 %) purchased from POCH (Avantor) was used as the precipitating agent for alumina and magnesia-alumina spinel preparation.

Gas reactants, including carbon dioxide, argon, and 2 % O_2 in a He mixture, were purchased from Linde, Poland. LDPE (low-density

polyethylene), polystyrene (PS), and polyethylene terephthalate (PET) samples were purchased from Sigma Aldrich. Plastic samples were purchased in the pellet form.

2.2. Synthesis of the catalysts

The synthesis of Ni-WC/Al$_2$O$_3$ and Ni-WC/MgWO$_4$/MgAl$_2$O$_4$ involved four steps.

a. preparation of Al$_2$O$_3$ or spinel MgAl$_2$O$_4$,
b. hydrothermal preparation of an organic-inorganic precursor,
c. carbothermal reduction,
d. passivation.

Spinel MgAl$_2$O$_4$ was prepared according to a procedure described previously in [65] via chemical precipitation in an alkaline solution. For the synthesis, Mg(NO$_3$)$_2$ and Al(NO$_3$)$_3$ were dissolved in deionized water at a Mg:Al molar ratio of 0.5. Then, the pH of the solution was adjusted to 10 with aqueous ammonia under vigorous stirring. The resulting suspension was aged for 24 h at 50 °C. Subsequently, the solid was separated, washed with deionized water, and dried at 100 °C to obtain a dry mass. The final step was calcination in air at 980 °C for 6 h. Al$_2$O$_3$ was obtained using the same route, but without magnesium nitrate.

To prepare the Ni-WC/MgWO$_4$/MgAl$_2$O$_4$ or Ni-WC/Al$_2$O$_3$ organic-inorganic precursors, appropriate amounts of AMT, nickel(II) nitrate, and glucose were dissolved in 120 cm^3 of deionized water and mixed for 0.5 h in a glass beaker to form a transparent solution. The solution was then transferred into a Teflon vessel, followed by the addition of the support (MgAl$_2$O$_4$ or Al$_2$O$_3$) and mixing for the next 0.5 h. Subsequently, a hydrothermal treatment at 180 °C for 24 h was conducted. Subsequently, the formed precursor was separated and dried under vacuum at 80 °C for 10 h. The next step involves carbothermal reduction. The dry precursor was placed in a tubular reactor made of stainless steel and de-aerated under Ar flow for 2 h at room temperature. Subsequently, the inlet and outlet valves were closed, and heating was initiated. The temperature was increased to 980 °C at a rate of 10 °C·min^{-1}). The annealing was performed at 980 °C for 6 h. The next step involved cooling to 40 °C at a rate of 10 °C·min^{-1}. The final step included passivation with 2 % O$_2$ in He gas mixture at 40 °C for 2 h.

2.3. Characterization of the catalyst

The catalysts were characterized before and after dry reforming. The phase composition was investigated using powder X-ray diffraction (XRD). A MiniFlex 600 diffractometer (Rigaku, Japan) equipped with Cu-Kα radiation was used for the measurements. XRD analysis was performed at room temperature with a scan rate of 0.01° in the 2θ range of 5–120°. The Scherrer constant was 0.891. For the analysis PDXL2 software was used. The obtained diffractograms were optimized using a pseudo-Voight function. The ICDD database was used for phase identification of the prepared catalysts.

Specific surface area (S$_{BET}$) and pore size distributions were investigated using N$_2$ sorption- desorption analysis at −196 °C. Nitrogen adsorption - desorption curves were obtained in the partial pressure p/p$_0$ range from 0.05 to 0.99. Calculations for specific surface area were based on Brunauer's, Emmet's and Teller's (BET) model in the approximate relative pressure (p/p$_0$) range from 0.05 to 0.3. Calculations for pore size distribution were performed using Barrett–Joyner–Halenda (BJH) model. Pore size distributions were derived based on the desorption isotherm branches. The total pore volumes were evaluated from the adsorbed amount of nitrogen at p/p$_0$ = 0.99 (the last adsorption point). Experiments were carried out using a NOVAtouch NT-LX-1 Autosorb iQ (Quantachrome Instruments). Prior to the measurements, the samples were dried and degassed for 5 h at 300 °C.

The morphology of the prepared catalysts was determined using scanning (SEM) and transmission (TEM) electron microscopy. For the SEM analyses, a FEi Quanta FEG 250 equipped with an EDS detector was used. Before analysis, the sample in the form of powder was placed on a stand covered with carbon tape. then, the samples were placed in the measurement chamber and evacuated to a high vacuum. For TEM measurements, Fei Tecnai G2 X-Twin and HR-TEM Fei Titan microscopes equipped with LaB6 and X-FEG guns were used. The sample preparation for TEM imaging included dispersing of the powder in absolute ethanol, applying the suspension to a carbon tape and evaporating the solvent.

Temperature-programmed carbon dioxide desorption (CO$_2$-TPD) and temperature-programmed reduction (H$_2$-TPR) were performed using an in-situ catalyst characterization system (ICCS) equipped with a thermal conductivity detector (PID Micromeritics). The analysis consisted of four steps. Firstly, around 0.1 g the catalyst sample was pre-treated at 300 °C under a helium stream. Next, the catalyst surfaces were saturated with CO$_2$ at 35 °C for 1 h under 20 % vol. CO$_2$ in a He stream (100 cm^3·min^{-1}). The third step involved the removal of physically adsorbed CO$_2$ under He flow (100 cm^3·min^{-1}) at 35 °C for 1 h. The final step involved monitoring the desorbed carbon dioxide in the temperature range of 35–850 °C under a He stream (100 cm^3·min^{-1}).

Temperature-programmed reduction (H$_2$-TPR) was investigated in the temperature range of 50–800 °C (heating rate 10 °C/min) under 10 % vol. H$_2$ in Ar flow (100 cm^3·min^{-1}). Before the reduction step, the catalyst sample (0.1 g) was pre-treated at 300 °C for 1 h under an argon flow (100 cm^3·min^{-1}). The experiments were carried out using were performed using an in-situ catalyst characterization system (ICCS) equipped with a thermal conductivity detector (PID Micromeritics).

X-ray Photoelectron Spectroscopy (XPS) experiments were carried out using a Specs UHV spectrometer (SPECS, Germany) equipped with a charge neutralizer. The binding energies were calibrated using the C 1 s peak at 284.8 eV as a reference. The collected data was analysed using CasaXPS software.

2.4. Catalytic activity in dry reforming of waste plastics

Pyrolysis combined with dry reforming of plastics (LDPE, PS, PET, and SWP) was performed in a two-stage reactor system (Fig. 1). The first stage consisted of a pyrolysis reactor (A) filled with 2 g of plastic sample. The plastic sample was places between two quartz wool layers. The second stage reactor (B) consisted of a reforming reactor filled with a catalyst bed (1 g) placed between quartz wool. The reactors were heated in two separate tube furnaces. The temperatures of the plastic and catalyst bed were controlled using a K-type thermocouple (06251189–41, B + B Thermo-Technik GmbH, Donaueschingen, Germany). Before the PCDR process, the reforming reactor was heated to 800 °C under constant argon flow. After reaching 800 °C on the catalyst bed, heating of the first-stage pyrolysis reactor was started. The pyrolysis reactor was then heated to 500 °C. After reaching 500 °C in the pyrolysis reactor, the temperature was maintained constant for 30 min. At the start of heating the first part of the system, carbon dioxide was fed into the system. The organic volatiles formed at pyrolysis step were directly transferred to the reforming reactor. The total amount of introduced carbon dioxide during the process was 8 g. The heating rate at both stages was 10 °C/min. After the reforming step, the products of the PCDR process were passed through a three-stage condenser system chilled room-temperature air (1), dry ice (2), and a mixture of water ice and dry ice (3) to trap any liquid products. The gas products were collected in a 25 L Tedlar bag and analyzed using a Clarus 590 gas chromatograph (PerkinElmer Inc., Waltham, MA, USA) equipped with Porapaq Q and Molecular Sieve 5 A columns and a TCD/FID detector. The efficiency of the PCDR process was measured as the yield of syngas generation (H$_2$, CO, and CH$_4$). Results labelled as No catalyst'' refer to experiments carried out without catalyst bed in the reforming unit (B). Instead of the catalytic bed, quartz wool was used, the same between which the catalyst was placed in the catalytic process.
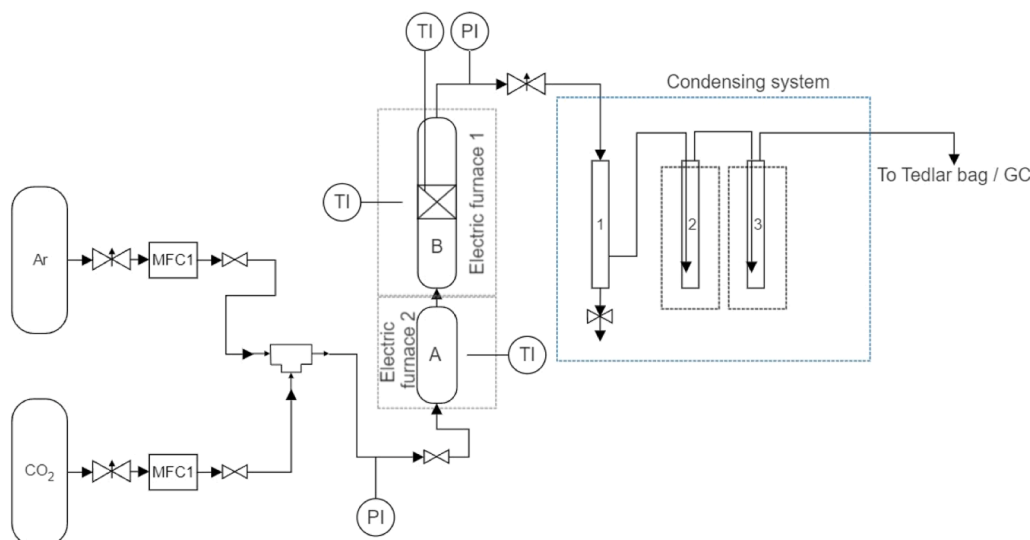
Fig. 1. Experimental system for two-stage PCDR (MFC- mass flow controller, TI- temperature indicator, PI- pressure indicator, A- pyrolysis reactor, B- reforming reactor)).

The contents of the liquid fraction and solid residue were determined based on the difference in masses before and after PCDR of the condensation vessels and pyrolysis reactor, respectively. The amounts of solid and liquid fractions as well as H_2, CO or CH_4 contents were expressed per 1 g of plastic sample. For gas products:

$$\frac{total \quad mmol \quad of \quad gas \quad produced}{mass \quad of \quad plastic} \quad \left[\frac{mmol}{g_P}\right]$$
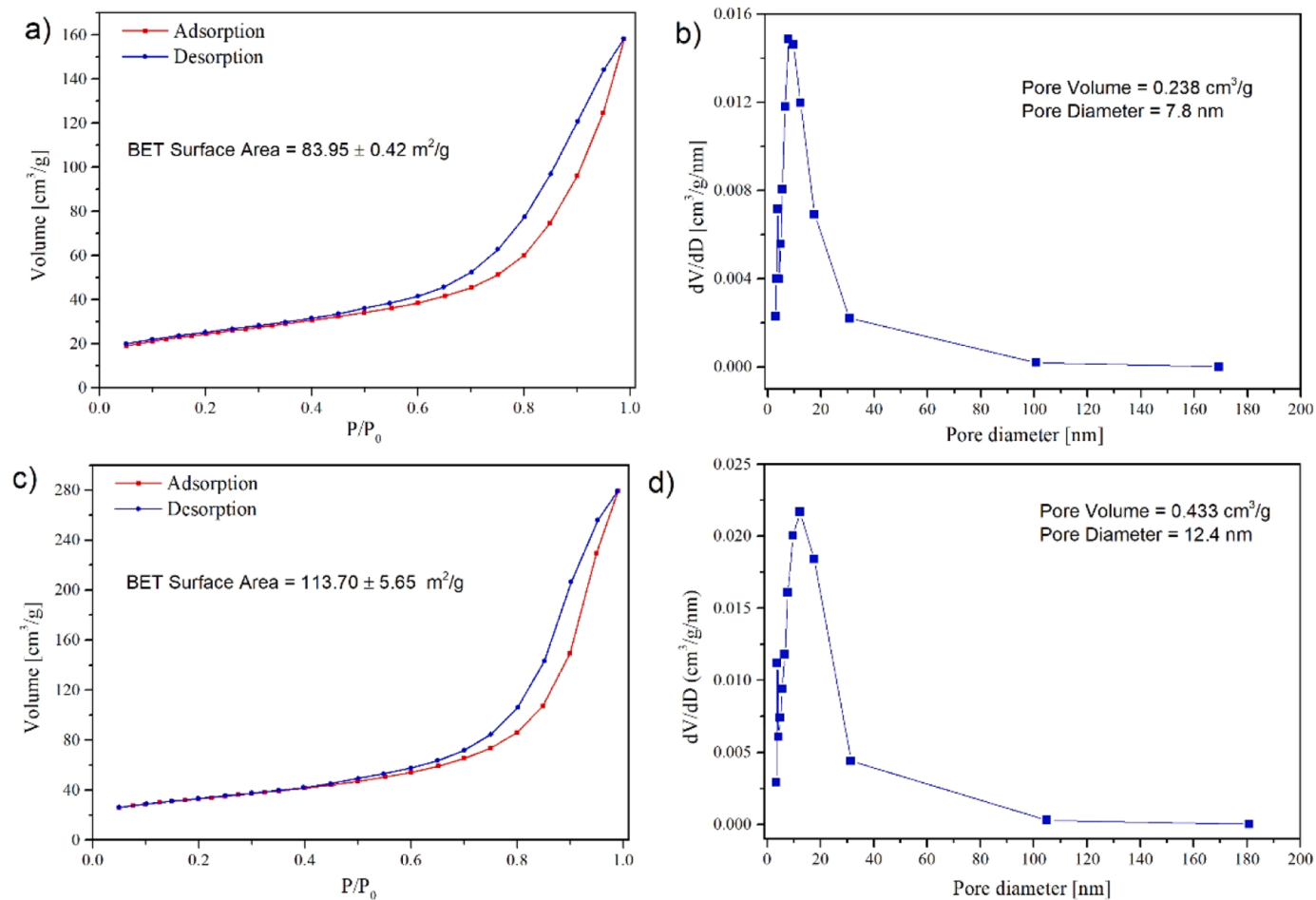
Fig. 2. a) Nitrogen sorption isotherms for Ni-WC/MgWO$_4$/MgAl$_2$O$_4$, b) BJH pore size distribution for Ni-WC/MgWO$_4$/MgAl$_2$O$_4$, c) Nitrogen sorption isotherms for Ni-WC/Al$_2$O$_3$ and d) BJH pore size distribution for Ni-WC/Al$_2$O$_3$.

For solid and liquid fractions:

$$\frac{total \quad mas \quad of \quad solid/liquid}{mass \quad of \quad plastic} \quad \left[\frac{g}{g_p}\right]$$

The H_2/CO ratio was calculated based on the formula:

$$n = H_{2out}/CO_{out},$$

Where:

H_{2out} – corresponds to the amount of hydrogen in outlet stream,
CO_{out} - corresponds to the amount of hydrogen in outlet stream.

3. Results and discussion

3.1. Characterization of catalysts before catalytic process

In Fig. 2a-d are presented a nitrogen adsorption-desorption isotherms and BJH pore size distributions for Ni-WC/MgWO$_4$/MgAl$_2$O$_4$ and Ni-WC/Al$_2$O$_3$ catalysts. The shape of the isotherm were classified as type IV according to the IUPAC classification [66]. The pore size for both catalysts were in the range 1–100 nm indicating the presence of meso and micropores. In the case of Ni-WC/MgWO$_4$/MgAl$_2$O$_4$ the majority of pore size was in the range of 2–30 nm. The maximum of pore size distribution plot was centered at 9.6 nm. For the Ni-WC/Al$_2$O$_3$ catalyst, the pore size distribution shifted slightly towards higher values. The maximum of the curve is observed at 12.4 nm. The Brunauer-Emmett-Teller (BET) surface areas of the Ni-WC/MgWO$_4$/MgAl$_2$O$_4$ and Ni-WC/Al$_2$O$_3$ catalysts were $83.95 \pm 0.42 \ m^2 \cdot g^{-1}$ and $113.70 \pm 5.65 \ m^2 \cdot g^{-1}$, respectively. The total pore volumes differed for particulate catalysts. For Ni-WC/MgWO$_4$/MgAl$_2$O$_4$ equaled 0.238 cm^3/g and for Ni-WC/Al$_2$O$_3$ was 0.433 cm^3/g.

The XRD patterns of the fresh and spent catalysts are shown in Fig. 3a) – b). The diffractograms of the catalyst before the PCDR process are shown in the first row. The reference patterns of particular compounds are included in Fig. S1 in the Supplementary Data. Both catalysts were characterized by a polycrystalline structure. The reflections attributed to WC were found at 2θ = 31.52°, 35.66°, 48.29°, 64.12°, 65.49°, 73.26°, 75.46 and 77.13° correspond to (0 0 1), (1 0 0), (1 0 1),(1 1 0), (0 0 2), (1 1 1), (2 0 0), (1 0 2) and (2 0 1) crystal planes, respectively (DB card no 1501588). The XRD peaks attributed to the nickel particles were observed at 2θ = 43.98° and 51.17° and were attributed to Ni (1 1 1) and Ni(2 0 0), respectively (DB card no 2102245, [67,68]). For the catalyst supported on Al$_2$O$_3$, peaks of weak intensity for γ-alumina were observed at 2θ = 39.5°, 46.1°, 66.9°, and 84.9°(DB card number 1010461). The Ni-WC/MgWO$_4$/MgAl$_2$O$_4$ catalyst peaks assigned to the MgAl$_2$O$_4$ support were identified at 2θ = 19.29°, 31.57°, 37.11°, 43.24°, 59.76°, 65.5°, 68.67°, and 77.5° (DB card no. 1010129). Reflections attributed to tungsten carbide peaks were observed at 2θ = 31.52°, 35.66°, 48.29°, 64.12°, 65.49°, 73.26°, 75.46°, and 77.13°, which were attributed to (0 0 1), (1 0 0), (1 0 1),(1 1 0), (0 0 2), (1 1 1), (2 0 0), (1 0 2), and (2 0 1), respectively (DB card no 1501588). For the Ni-WC/MgWO$_4$/MgAl$_2$O$_4$ catalyst, except the XRD peaks attributed to Ni, WC, and MgAl$_2$O$_4$ phases, additional reflections assigned to the MgWO$_4$ phase at 2θ = 18.87°, 23.85°, 24.5°, 30.43°, 30.73°,36.44°, 41.62°, and 61.73° correspond to the (1 0 0), (0 1 1), (1 1 0), (1 1 −1), (0 0 2), (1 2 −1), and (1 1 3) crystal planes, respectively were observed (DB card no. 1010642, [69]). The magnesium tungstate phase was a result of solid state reaction between MgO and WO$_3$ formed in the intermediate precursors according to the equation [69]:

$$MgO(s) + WO_3(s) \rightarrow MgWO_4(s) \tag{1}$$

The formation of alkali tungstate was reported by Li et al. [47,70]. They prepared cobalt-based catalysts with WC-activated carbon support. They noted a formation of low content of CaWO$_4$ phase due to reaction of WC and calcium oxide CaO present in the activated carbon material.

The average crystalline sizes towards Ni (111) and WC (100) directions were determined based on the Scherrer formula. The crystalline size of nickel significantly differed for particular catalysts. The WC crystalline sizes were similar. For Ni-WC/MgWO$_4$/MgAl$_2$O$_4$ catalyst
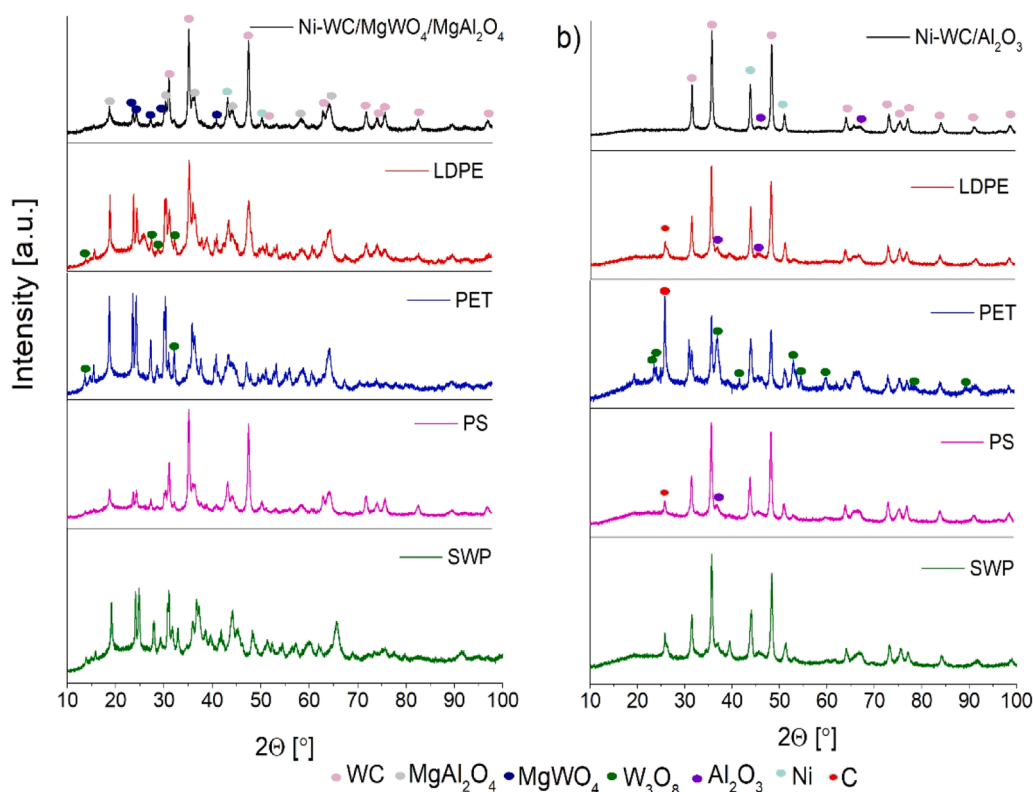

Fig. 3. XRD pattern of fresh and spent a) Ni-WC/MgAl$_2$O$_4$/MgAl$_2$O$_4$ and b) Ni-WC/Al$_2$O$_3$ catalysts.

average crystalline sizes for Ni and WC equalled 16.0 nm and 25.6 nm, respectively. In the case of Ni-WC/Al$_2$O$_3$ catalyst crystalline size for Ni was equal to 26.5 nm and for WC 29.0 nm.

The morphology of the catalysts was determined using scanning and transmission electron microscopy. In Fig. 4 are presented SEM images (Fig. 4b)- e)) and results of SEM-EDX analysis for the Ni-WC/MgWO$_4$/ MgAl$_2$O$_4$ catalyst elemental composition (Fig. 4a)). The nickel content determined by EDX equaled 6 wt %, while the content of W, Al, Mg, O and C were determined as ~29 wt %, ~21 wt %, ~7 wt %, ~23 wt % and 14 wt %, respectively. The morphology observed for this catalyst was characterized by an even distribution of structures with higher contrast (brighter points visible in the images) in a continuous phase with lower contrast. The obtained structures with higher contrast were tungsten carbide and nickel particles deposited on and surrounded by an amorphous carbon matrix. The formation of core-shell structures composed of metal carbide and amorphous carbon as the core and shell,

respectively, has been reported in the literature. Under hydrothermal treatment, glucose undergoes chemical transformations, leading to hydrothermal carbonization through dehydration and polycondensation-polymerization. Falco et al. [2] investigated the mechanism of hydrothermal carbons using i.a. glucose. They stated that the first step included the dehydration of glucose molecules, leading to the formation of mainly 5-hydroxymethylfurfular (HMF), leviunic acid, dihydroxyacetone, and formic acid. It then proceeds through polymerization reactions, resulting in the formation of polyfuranic type compound. When higher temperatures (above 180 °C)are applied, the polyfuanic chains undergo intermolecular condensation, dehydration, and decarboxylation, leading to aromatization. The degrees of dehydration and decarboxylation depend on the synthesis conditions. According to Titirici et al. [3],the formed precursor takes the shape of spheres terminated with hydrophilic–OH and–COOH groups. The metal ions present in the reaction medium interact with hydrophilic groups and are deposited on
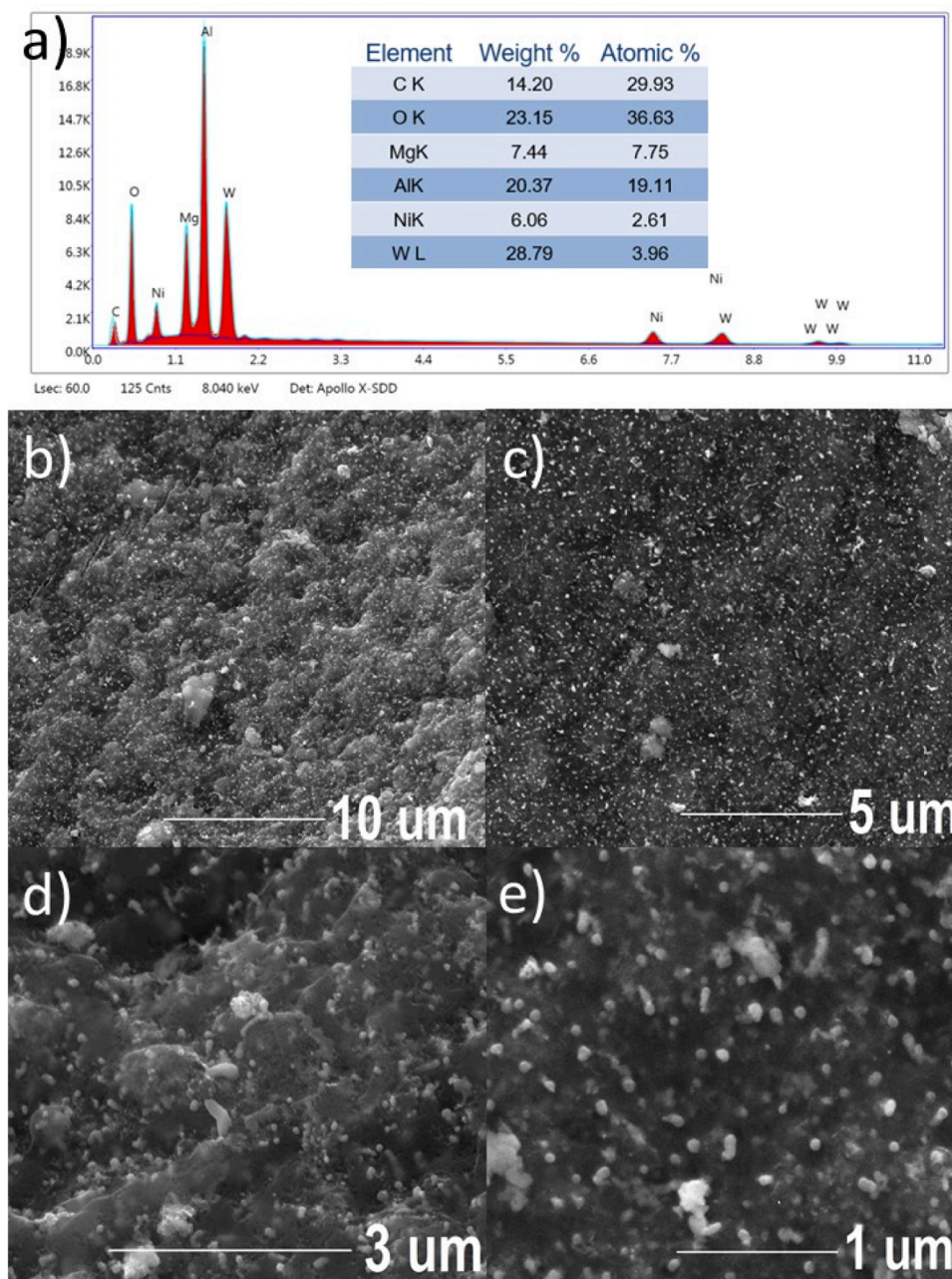

Fig. 4. a) EDS analysis, b)- e) SEM images of Ni-WC/MgWO$_4$/MgAl$_2$O$_4$ catalyst.

the surface of the carbon spheres. In the presence of metal ions including tungsten high-temperature annealing in an inert atmosphere results in the formation of metal carbide particles embedded in a carbon matrix [71–74]. The amorphous character of carbon is in agreement with XRD results (see Fig. 3). Quantitative analysis of elemental composition was also performed for Ni-WC/Al$_2$O$_3$. The content of Ni, W, C, O and Al equaled ~7 wt %, ~27 wt %, ~18 wt %, ~25 wt % and ~23 wt %, respectively.

To further investigate the morphology and distribution of particular catalyst components, STEM/TEM analyses were performed (Fig. 5 and Fig. 6). For Ni-WC/MgWO$_4$/MgAl$_2$O$_4$ catalyst despite all phases identified using XRD method including Ni, WC, MgAl$_2$O$_4$ and MgWO$_4$ were observed. The nickel particles based on SAED/FFT (selected area electron diffraction/ fast Fourier transform) analysis were identified as spherical particles up to 100 nm in size. The map for nickel particles did not completely coincide with the map for tungsten. The map obtained for nickel shows partial deposition on tungsten carbide and partly on the MgAl$_2$O$_4$ spinel. The distribution map for carbon did not overlap completely with the position of the tungsten signals. The images show areas where unbound carbon is visible (Fig. 5a) - b)).

In the case of Ni-WC/Al$_2$O$_3$, particles consisting of tungsten and nickel were deposited on the Al$_2$O$_3$ surface (Fig. 5a) and b)). The distribution of carbon corresponded to the distribution of tungsten element indicating the formation of WC particles. The FFT analysis was performed to confirm formation of WC. The determined interplanar spacings equalled 0.25 nm and 0.28 nm and were attributed to WC (100) and (001) crystal planes, respectively.

Temperature programmed carbon dioxide profiles (CO$_2$-TPD) are presented in Fig. 7. The profile lines were similar for both the catalysts. Four desorption peaks can be distinguished, indicating four types of active sites. The first one (I), which is the most prominent, is characterized by a maximum at approximately 150 °C, indicating weak basic sites. The subsequent desorption peaks were different for the catalysts. In the case of desorption peak II, the temperatures were 420 °C and

370 °C for Ni-WC/MgWO$_4$/MgAl$_2$O$_4$ and Ni-WC/Al$_2$O$_3$, respectively. The III CO$_2$ desertion peak for Ni-WC/MgWO$_4$/MgAl$_2$O$_4$ was observed at 420 °C, while of Ni-WC/Al$_2$O$_3$ was slightly shifted to lower temperature (410 °C). The IV desertion peak. The last IV desorption peak was observed at 800 °C for both the catalysts. The catalysts differ in terms of desorbed carbon dioxide. The amounts of CO$_2$ were estimated from integration of CO$_2$-TPD peaks. For Ni-WC/Al$_2$O$_3$ and Ni-WC/MgWO$_4$/MgAl$_2$O$_4$ catalysts 0.197 mmol/g$_k$ and 0.231 mmol/g$_k$ of desorbed carbon dioxide were observed.

Fig. 8 represents temperature programmed reduction (H$_2$-TPR) profiles. The profiles were similar for both catalysts indicating the presence of comparable species. The graphs show one high-intensity peak at approximately 680 °C and 650 °C for the Ni-WC/MgWO$_4$/MgAl$_2$O$_4$ and Ni-WC/Al$_2$O$_3$ catalysts, respectively. The profiles also showed three reduction peaks in the temperature range below 500 °C. The reduction peaks can be attributed to the reduction of NiO and tungsten oxide phases formed during passivation step [75]. The catalyst supports including Al$_2$O$_3$, MgWO$_4$, and MgAl$_2$O$_4$ are not reducible under these conditions.

3.2. Characterization of spent catalysts

The XRD patterns of the spent catalysts are presented in Fig. 3a) and b). The reference patterns of MgWO$_4$, W$_3$O$_8$, WC, Ni, C, Al$_2$O$_3$, and MgAl$_2$O$_4$ are shown in Figure. S1 (see Supplementary Data). In the case of the Ni-WC/MgWO$_4$/MgAl$_2$O$_4$ catalyst after the polystyrene PCDR process, the XRD pattern is similar to those of the fresh catalyst. In the diffractogram, only Ni, WC, MgWO$_4$, and MgAl$_2$O$_4$ phases were identified. However, the patterns of spent catalyst after the PCDR process of PET, SWP, and LDPE significantly differed from the pattern for the fresh catalyst. The XRD reflections attributed to MgWO$_4$ become more intense and visible at 2θ = 15.8°, 19.05°, and 24. 02°, 24.75°, 30.63°, 36.63°, 41.68° and 61.73°. Moreover, new reflections attributed to the W$_3$O$_8$ (DB card numbers 2101049 and 2101050) phases were identified at 2θ
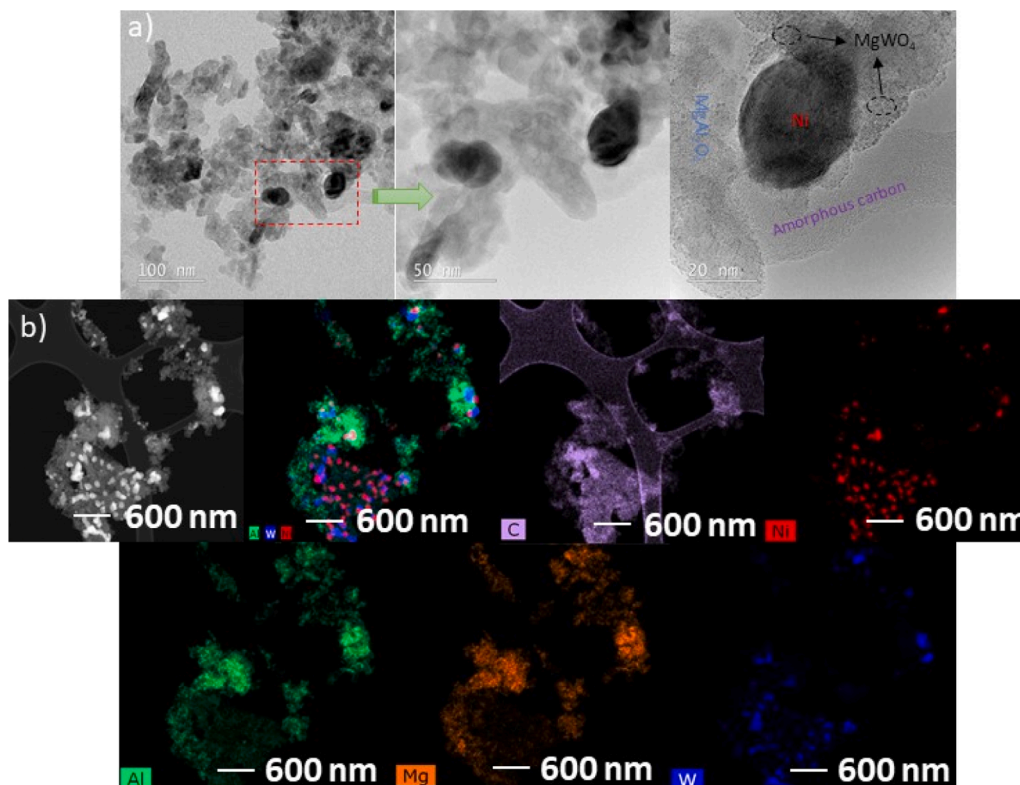

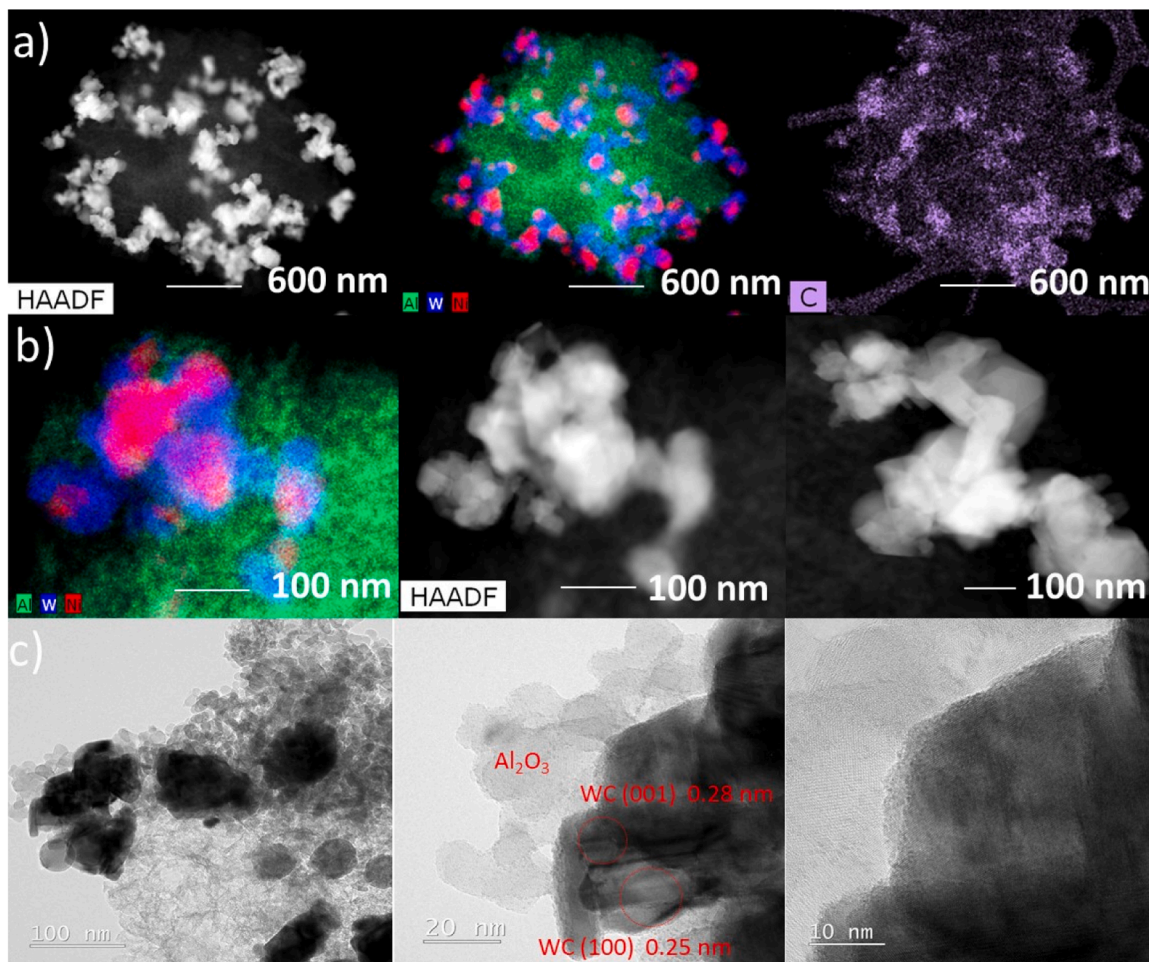**Fig. 5.** a) TEM images and b) HAADF and EDS mapping of Ni-WC/MgWO$_4$/MgAl$_2$O$_4$ catalyst.

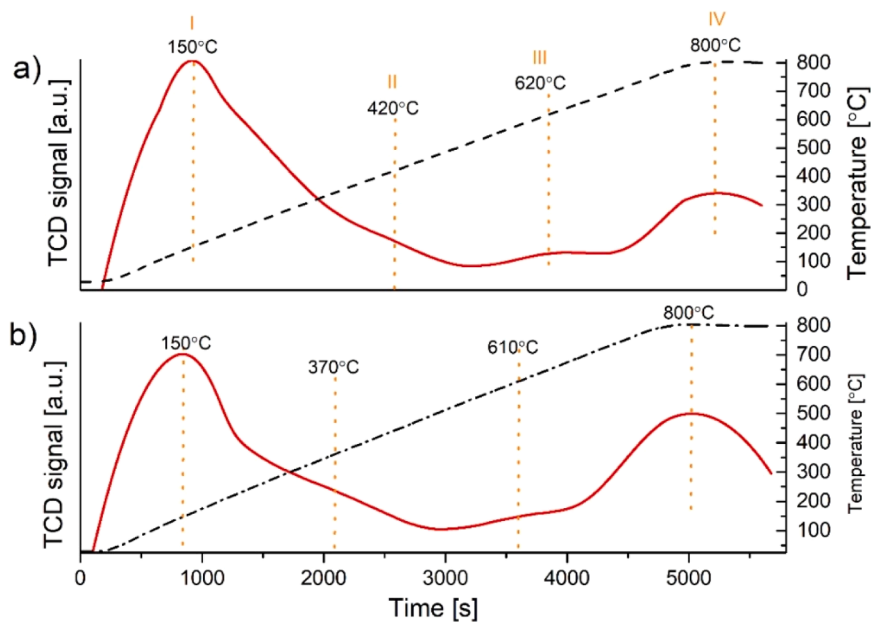**Fig. 6.** a) -b) HAADF images and EDS mapping, c) TEM images of Ni-WC/Al$_2$O$_3$ catalyst.

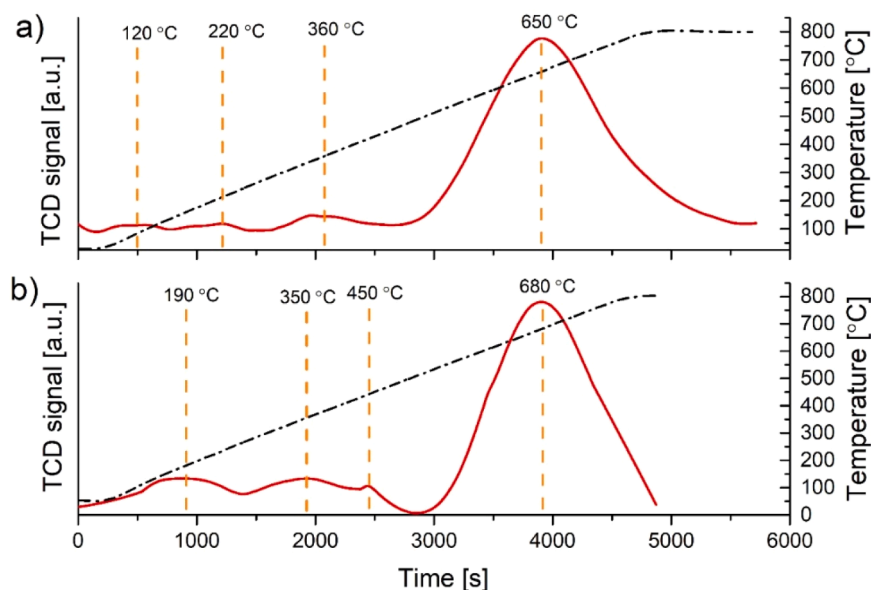**Fig. 7.** CO$_2$-TPD profiles for a) Ni-WC/MgWO$_4$/MgAl$_2$O$_4$ and b) Ni-WC/Al$_2$O$_3$.

Fig. 8. H_2-TPR profiles of a) Ni-WC/Al$_2$O$_3$ and b) Ni-WC/MgWO$_4$/MgAl$_2$O$_4$.

$= 13.70°$, $27.65°$, $28.99°$, and $32.64°$. The enhancement of the visibility and intensity of the XRD peaks assigned to MgWO$_4$ and W$_3$O$_8$ corresponds to the weakening of the WC signal, indicating oxidation of the carbide phase. The reflection at $2\theta = 19.05°$ can be classified as both MgWO$_4$ and W$_3$O$_8$ phases owing to the overlapping of the signals. Weak and broad peaks in the 2θ range above $35°$ were identified, and overlapped signals for MgWO$_4$ and W$_3$O$_8$ were observed. The formation of the oxidized forms of tungstate, that is, MgWO$_4$ and W$_3$O$_8$, as well as the disappearance of the WC phase, correlated with the properties of the plastic used as feedstock. In the case of polystyrene, the structure of the catalyst was preserved. The oxygen content based on CHNS analysis reported in [48] was the lowest for PS (2.434 ± 0.122 wt %). The highest oxygen content was observed for PET plastic, which was a result of the presence of oxygen atoms in the main chain. For the spent catalysts after the PCDR process using this plastic, the oxidation of WC was the most prominent. In the case of LDPE the oxygen content was approximately 6 wt %. Low-density polyethylene is known for its branched structure, and thus, a higher content of unpolymerized

terminal groups that can be oxidized. The spent catalyst after PCDR of LDPE also underwent oxidation, but to a lesser extent than in the case of PET. After the PCRD process of the simulated waste, the XRD pattern of the Ni-WC/MgWO$_4$/MgAl$_2$O$_4$ partial phase transformation to MgWO$_4$ was observed. In the case of the Ni-WC/Al$_2$O$_3$catalyst, the oxidation of WC to W$_3$O$_8$ was observed. However, in contrast to the Ni-WC/MgWO$_4$/MgAl$_2$O$_4$ catalyst, reflections attributed to graphitic carbon were observed for the Ni-WC/Al$_2$O$_3$ catalyst after the PCDR of each type of plastic. The most prominent peak was observed for poly(ethylene terephthalate).

To investigate the surface composition of the catalysts and changes after the PCDR processes, XPS analysis was performed. The analysis was performed on fresh and spent catalysts after dry reforming of LDPE. Fig. 9 shows the XPS spectrum of the tungsten 4f region. In the case of the fresh Ni-WC/Al$_2$O$_3$catalyst, three peaks were observed after the deconvolution of the W 4f region. The first and second peak at 38.6 eV and 36.4 eV are forming the doublet indicating the presence of W^{6+} species attributed to tungsten trioxide. The third peak, with a maximum
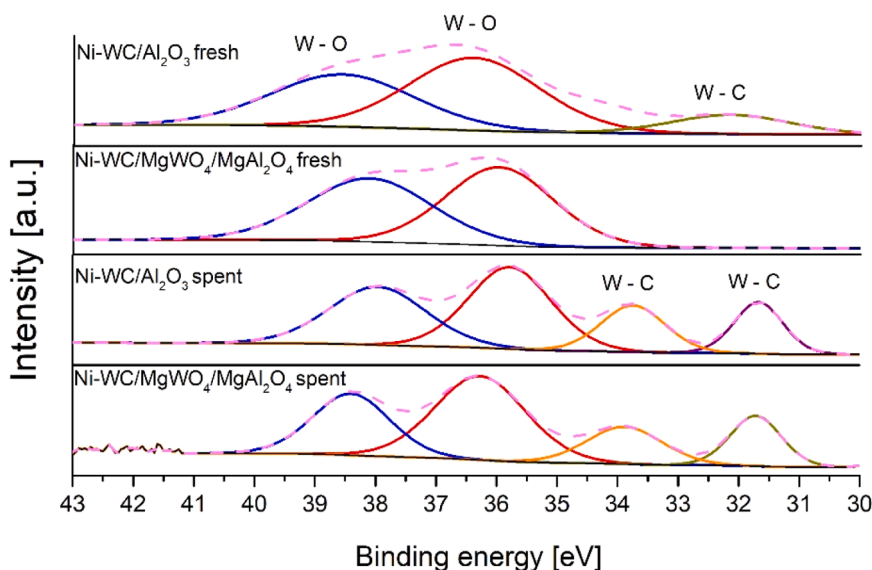

Fig. 9. XPS spectra of W 4f region for fresh and spent catalysts.

at 32.1 eV is assigned to W-C bonding. For the Ni-WC/MgWO$_4$/MgAl$_2$O$_4$ catalyst, only a doublet corresponding to WO$_3$ was observed. The presence of tungsten oxides on the surface results from the passivation step used during the synthesis of the catalyst. The absence of a signal attributed to the tungsten carbide phase results from surface coverage with unbonded carbon, which is in agreement with the TEM analysis. Comparing the XPS spectra of the tungsten 4f region of the catalysts after the catalytic process, similar profiles, consisting of two doublets, were observed. The first corresponds to W^{6+} (WO$_3$) and the second corresponds to WC. The coexistence of both phases indicates the occurrence of oxidation and carburization cycle characteristic of the metal carbides [76,77].

The plots representing the carbon 1 s region are presented in Fig. 10. For Ni-WC/Al$_2$O$_3$, a broad peak from 289 eV to 280 eV, attributed to C-C bonding, was observed. For Ni-WC/Al$_2$O$_3$, the peak was extensive, covering regions associated with sp^2, sp^3, WC, and oxidized forms of carbon. For the Ni-WC/MgWO$_4$/MgAl$_2$O$_4$ sample, the main peak is narrower, indicating the presence of sp3 hybridized carbon. In the case of spent catalysts the C 1 s plots are very similar. The signal was deconvoluted into three peaks centered at 289.0 eV, 284.9 eV and 284.3 eV. The peaks were assigned to carboxyl and carbonyl O= C–OH, C=O, C=C (sp^2), and C-C (sp^3), respectively. They are distinguished from catalysts before the catalytic process by the presence of a peak at 284.3 eV, which is attributed to sp^2 hybridized graphitic carbon (C=C). Therefore, these results indicate the formation of graphitic carbon deposits on the catalyst surface. No peak assigned to carbide was observed due to attenuation of the signal by the graphitic overlayers [50,76,78].

Fig. S2 represents the XPS O 1 s spectra. For catalyst before PCDR process single broad peak attributed to oxygen bonded with is observed. For spent catalysts second peak at higher binding energies (533.1 eV and 533.5 eV) was observed. The second peak results from oxygen species bonded with organic carbon. XPS spectra for the rest elements: Al 2p, Ni 22 g and Mg 2 g are presented in Supplementary data (Figs. S3–5). The spectra before and after catalytic process and similar. Binding energies for particular elements correspond to Al-O, Mg-O and Ni-O bonds.

Fig. 11 shows the TG and DTG profiles of the catalysts before the catalytic reaction and after the PCDR of the individual plastics and their mixtures. For catalysts before the catalytic process, weight loss is visible as a result of the oxidation of amorphous carbon present after synthesis. For the Ni-WC/MgWO$_4$/MgAl$_2$O$_4$ catalyst, the observed weight loss was 7.5 %. The mass loss DTG peak is in the range of 380–550 °C with a peak

maximum of approximately 490 °C. The temperature range of the loss indicated the oxidation of amorphous carbon and WC in the catalyst sample. In the case of the Ni-WC/Al$_2$O$_3$ catalyst, the weight loss was higher, amounting to approximately 17 % by weight. The maximum of the peak shifted slightly towards higher temperatures, with a maximum of 530 °C. For both catalyst samples before the catalytic process, an increase in mass after the oxidation of carbon, tungsten carbide to tungsten oxide and nickel to nickel oxide was visible at approximately 590 and 610 °C for Ni-WC/MgWO$_4$/MgAl$_2$O$_4$ and Ni-WC/Al$_2$O$_3$, respectively. For the TG/DTG profiles of the samples after the PCDR processes, there is a visible difference in the mass loss and position of the DTG peak. Among the samples after the catalytic process, the maximum DTG peak occurring at the lowest temperature was observed for the samples after polystyrene reforming. For both catalysts, the maximum was observed at approximately 550 °C. Carbon oxidation in this temperature range indicated the presence of amorphous filamentary carbon [41]. The highest values of mass loss and the location of the DTG peak maximum were observed for the catalysts after the dry reforming of low-density polyethylene. For the catalysts after PCDR LDPE, two peaks are visible. The first is around 600 °C and the second is at approximately 650 and 700 °C for Ni-WC/MgWO$_4$/MgAl$_2$O$_4$ and Ni-WC/Al$_2$O$_3$, respectively. The obtained results indicate the formation of carbon deposits corresponding to carbon with a more ordered structure - graphite carbon [19,41,79]. The lowest mass losses for both catalysts were observed after the dry reforming of the PET plastic. This is because plastics are characterized by the highest proportion of solid residue in the pyrolysis reactor. In addition, this is due to the fact that the structure of the PET polymer has the highest content of oxygen in the form of carboxyl groups, which is conducive to the additional generation of various forms of oxygen, and thus the oxidation of the carbide fraction. Therefore, as a result of oxidation during the catalytic process, the mass loss visible in the TG profile was the smallest. The obtained results are in agreement with the XRD results. For samples after the PCDR PET process, the largest tungsten oxide fraction was observed in the XRD spectrum. All assays also showed a low-intensity peak in the temperature range of 25–150 °C associated with moisture loss. The type of plastic and, therefore, the characteristics of the pyrolysis volatiles affected the type of deposited carbon. For the PCDR process carried out for the LDPE feedstock, which decomposes into aliphatic saturated and olefinic chains, a higher proportion of graphitic carbon was observed in the DTG profiles. In the case of the spent catalysts after the PET and PS processes,
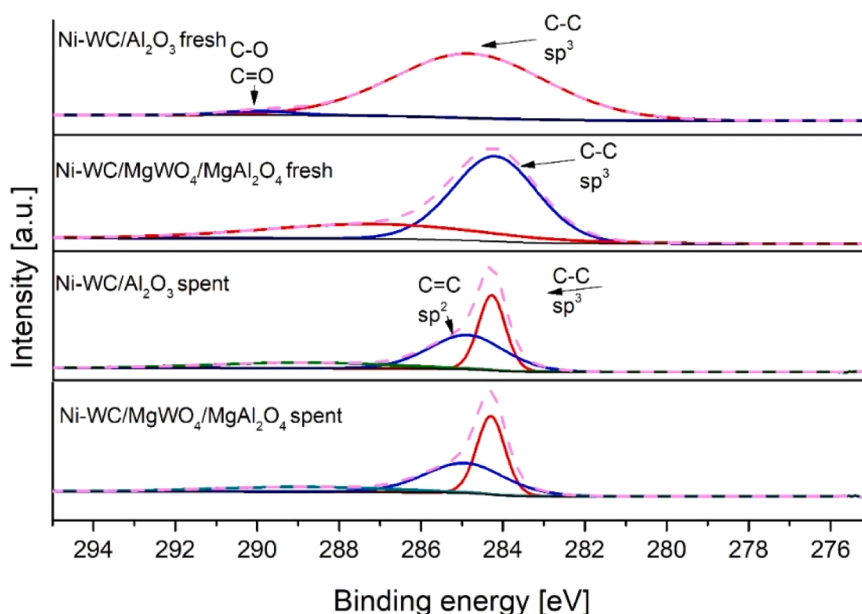

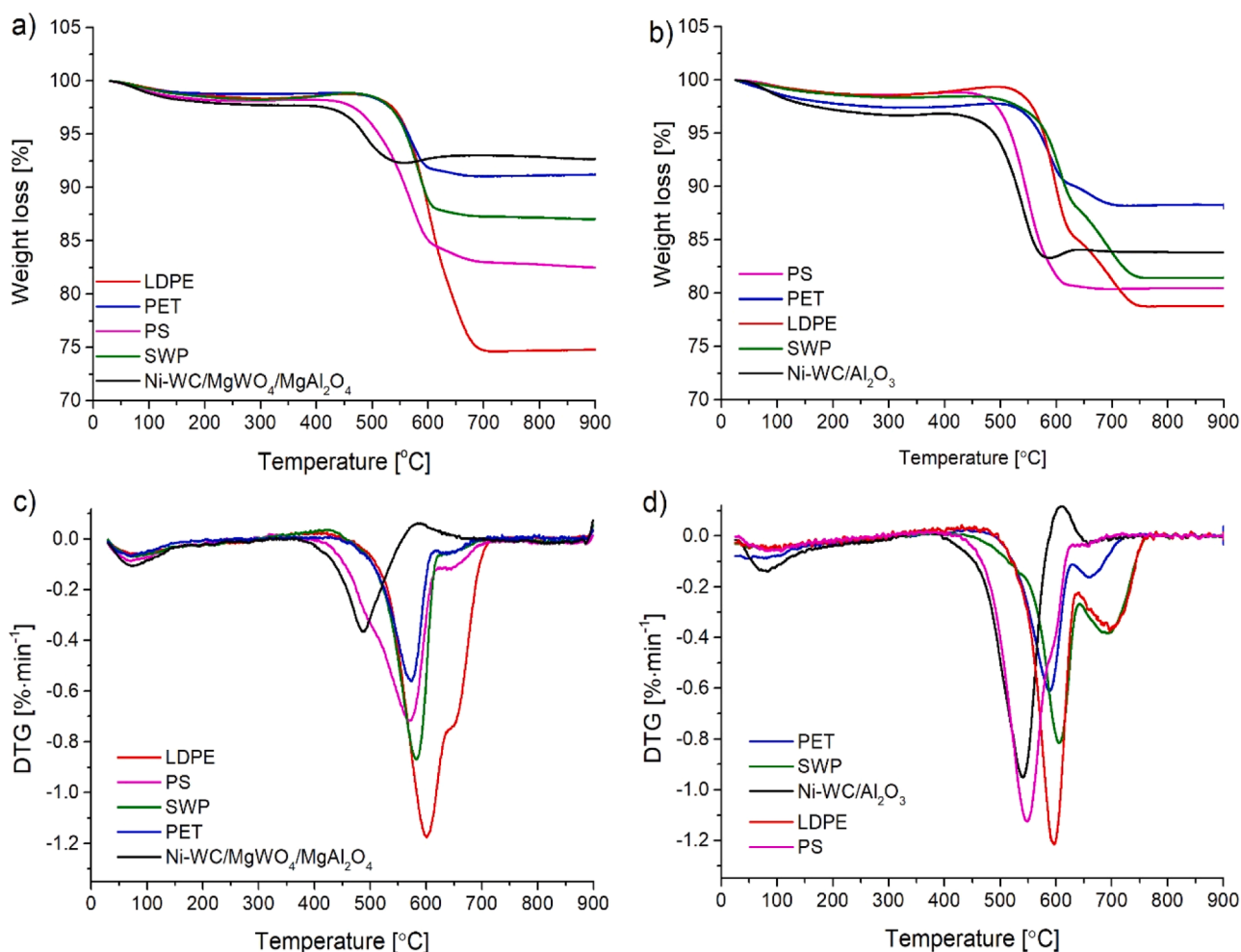**Fig. 10.** C 1s XPS spectra for fresh and spent catalysts.

Fig. 11. TG profiles of fresh and spent a) Ni-WC/MgWO$_4$/MgAl$_2$O$_4$ and b) Ni-WC/Al$_2$O$_3$, DTG profiles of c) Ni-WC/MgWO$_4$/MgAl$_2$O$_4$ and d) Ni-WC/Al$_2$O$_3$ catalyst.

the DTG peaks shifted towards the temperatures assigned to filamentous and encapsulating carbon. It should also be mentioned that the types and impurities present in the feedstocks result in different catalyst deactivation. In real-life feedstocks used in pyrolysis additional impurities including sulphur, ammonia or chloride compounds affect the way of catalyst structural changes through sintering and blocking of metal active sites by deposition of fine particles or chemical bonding [80,81].

3.3. Catalytic activity

The plastic samples used in the experiment are characterized in [48]. Data for the TG/DTG profiles are available in [82]. All examined plastic samples under inert conditions are decomposed up to 460°C. For polystyrene and low-density polyethylene underwent almost complete removal and volatilization. In the case of PET material solid residue at level of 52.55 wt %. was observed. The main DTG peaks were similar for the examined plastic samples and equalled 448°C, 403°C and 414°C for LDPE, PD and PET, respectively. Plastic samples are built from hydrogen and carbon; however, oxygen was also detected. The origin of oxygen results from the slight atmospheric oxidation of unpolymerized terminal groups and the presence of hydroxyl groups resulting from moisture. The presence of oxygen in plastic samples has also been reported previously [22]. Plastics differ in their chemical structure:

- LDPE – constructed with branched alkane chains. Owing to the branched structure of LDPE and the possible high level of unpolymerized groups, relatively high levels of oxygen may be present in

the polymer structure. The oxygen content determined by the CHNS analysis was 6.552 ± 0.328 wt % [48]. During pyrolysis process LDPE is decomposed to short-chain hydrocarbons, mainly alkenes [83],
- PS – composed of ethyl chains with phenyl substituent. During the pyrolysis the generated hydrocarbons are composed mainly to aromatic compound such as styrene, toluene and its dimers [7]. In our study the content of oxygen in the PS sample was the lowest and equaled 2.434 ± 0.122 wt %. [48].
- PET – The PET structure includes alternating ethyl and terephthalic chains. The oxygen content was the highest among the examined samples, reaching 27.977 ± 1.399 wt %. During the pyrolysis of PET significant solid fraction is produced as well as carbon oxides due to the decarboxylation of terephthalic units [48,84,85].

In Figs. 12 and 13 are presented results of the PCDR processes in the presence and absence of the catalyst in the reforming unit The product distribution was differentiated depending on the type of plastic and the catalyst used. The efficiency of gaseous product generation was inversely proportional to the production of the liquid and solid fractions. The highest amounts of liquid and solid fractions were observed in experiments processed with polystyrene and polyethylene terephthalate, respectively. In the case of PET, nearly 50 % of the starting plastic sample was converted to char and residue in the first reactor. For SWP, the proportion of solid residue corresponded to the amount of PET in the starting plastic mixture. For the low-density polyethylene and polystyrene plastics, virtually no solid residue was observed. The obtained
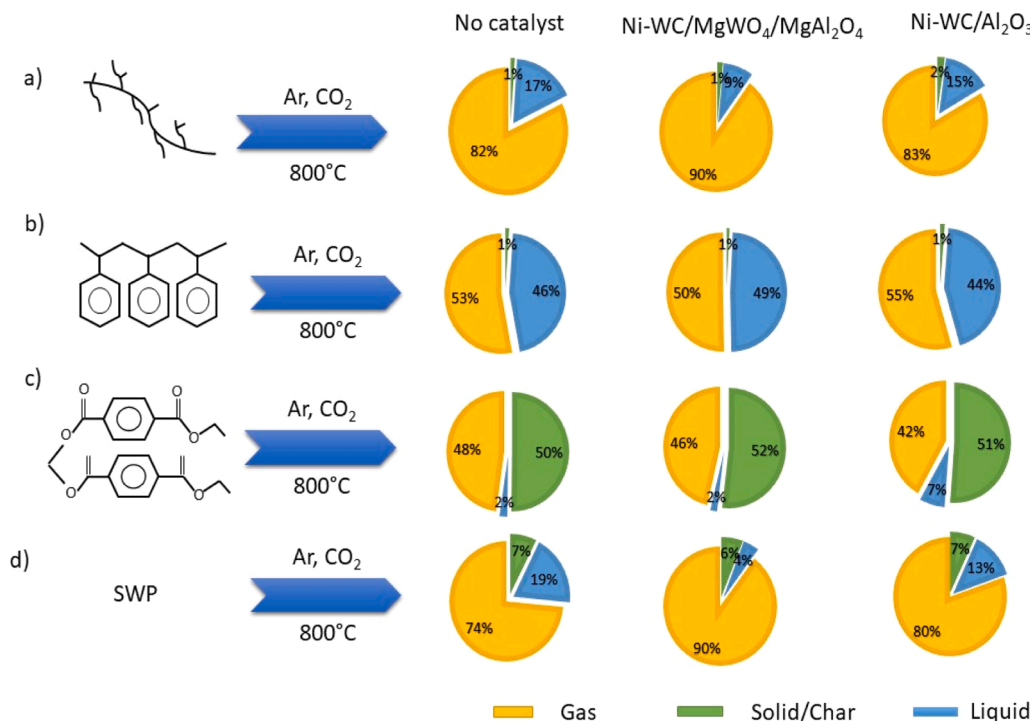
Fig. 12. Distribution of gaseous, liquid and solid fractions after the catalytic and non-catalytic PCDR process.
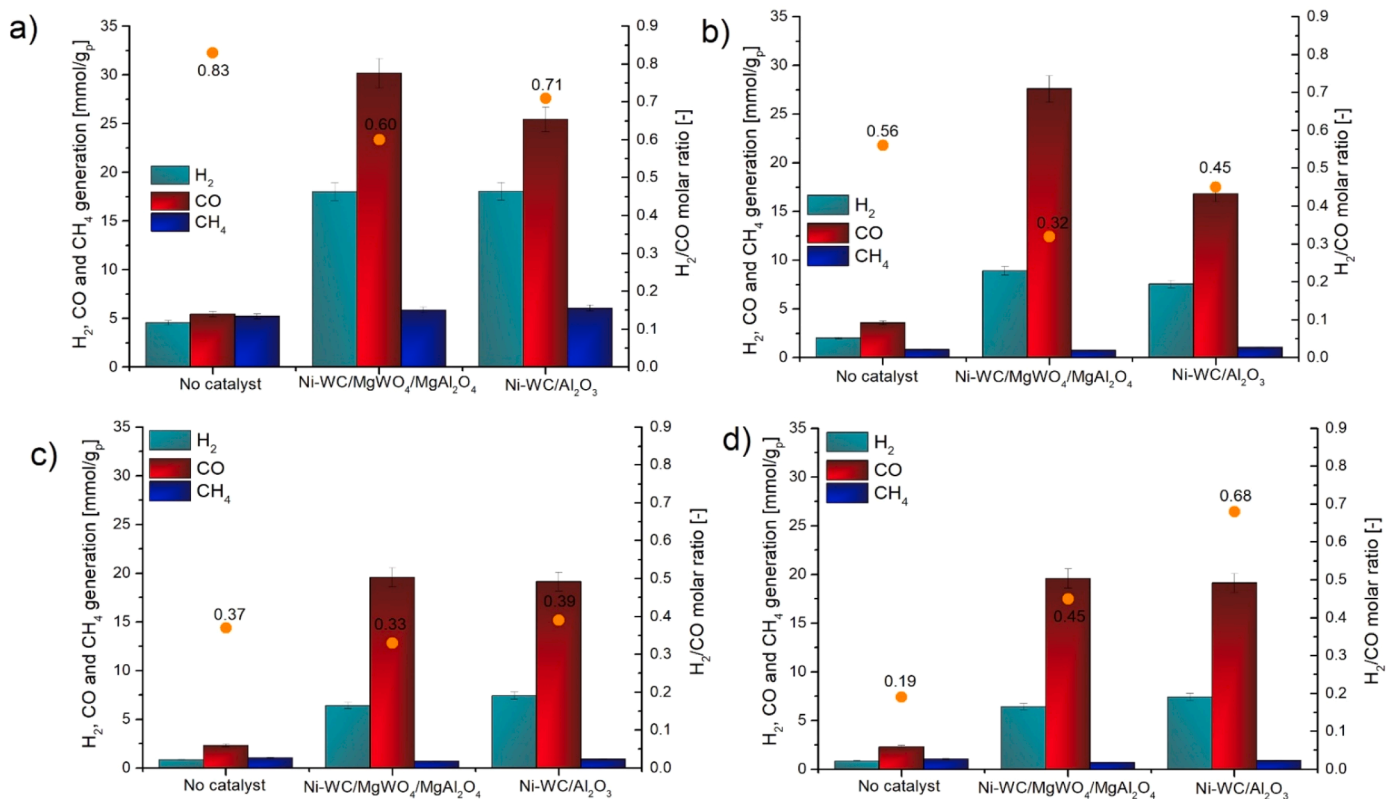
Fig. 13. Distribution of gas for PCDR of a) low-density polyethylene, b) polystyrene, c) polyethylene terephthalate and d) simulated waste.

results for the solid residue are in agreement with the TG profiles for the plastic samples. The highest yields of liquid fraction ranging from 0.49 g/gp to 0.46 g/gp were observed for process carried out with polystyrene. Similar results were obtained by Saad and Williams [22].

They investigated the effects of different plastic types (LDPE, HDPE, PP, PS, and PET) on product distribution in a two-stage PCDR system. They also observed the highest level of solid residue for the PET plastic and the highest content of gas products for the LDPE sample. Alvarez et al.

[86] investigated the effect of plastic type on hydrogen production during pyrolysis combined with steam reforming. They found that olefinic products formed during the pyrolysis of materials such as polypropylene and polyethylene were easily decomposed at 800 °C, forming more hydrocarbon light species, resulting in a higher gas fraction content. On the contrary, during the pyrolysis of polystyrene aromatic compounds such as styrene, toluene, and its dimers formation has been reported [87]. Gaseous pyrolytic products composed of olefinic compounds have been reported to be more susceptible to decomposition than aromatic compounds because of their lower C-C bond energy [15, 83,85]. Among other polymers, the PET sample is distinguished by the presence of heteroatom oxygen in the main chain, resulting from the presence of COO- groups. During the pyrolysis and reforming steps, they undergo decarboxylation, which leads to higher CO and CO_2 contents in the outlet streams. Moreover, CO may be formed by the reaction between CO_2 and char [24]. The highest amounts of generated gas were observed for the processes carried out with low-density polyethylene and simulated waste. The high level of gas products in the outlet stream observed for simulated waste resulted from a dominant share of plastics with aliphatic unsaturated chains (PP, HDPE, and LDPE). Among the gas products, saturated and unsaturated hydrocarbons, as well as syngas components, including H_2 and CO, are released. Table 1 and Fig. 10 summarize the results of the quantitative analysis of methane, hydrogen, and carbon monoxide generation. In all processes, the syngas generation yields were higher for processes carried out in the presence of catalysts than for uncatalyzed processes.

The highest efficiency in synthetic gas generation was observed in the case of PCDR of low-density polyethylene carried out with the Ni-WC/MgWO$_4$/MgAl$_2$O$_4$ catalyst. The sum of generated hydrogen and carbon monoxide was equal to 48.20 ± 2.41 mmol per 1 g of plastic. The amounts of syngas components were 18.05 ± 0.39 mmol/g$_p$ and 30.19 ± 1.51 mmol/g$_p$ for H_2 and CO, respectively. The syngas (H_2 + CO) yield for process without any catalyst was nearly five times lower (10.00 ± 0.51 mmol/g$_p$). For Ni-WC/Al$_2$O$_3$ catalyst the amount of generated hydrogen was similar to Ni-WC/MgWO$_4$/MgAl$_2$O$_4$ catalyst and equalled 18.01 ± 0.91 mmol/g$_p$. For PCDR of polystyrene generated hydrogen equalled 8.93 ± 0.45 mmol/g$_p$ and 7.56 ± 0.38 mmol/g$_p$ for Ni-WC/MgWO$_4$/MgAl$_2$O$_4$ and Ni-WC/Al$_2$O$_3$, respectively. During PCDR of simulated waste the H_2 generation yields was 12.57 ± 0.61 mmol/g$_p$ and 12.00 ± 0.58 mmol/gp for Ni-WC/MgWO$_4$/MgAl$_2$O$_4$ and Ni-WC/Al$_2$O$_3$, respectively. The differences in activity between the catalysts are the most prominent in terms of carbon monoxide generation. Exemplary, for Ni-WC/MgWO$_4$/MgAl$_2$O$_4$ catalyst the CO yield in PCDR of LDPE was 30.19 ± 1.51 mmol/g$_p$, while for Ni-WC/Al$_2$O$_3$ equalled 25.44 ± 1.27 mmol/g$_p$. A greater variation in carbon monoxide generation for both catalysts was observed at the PCDR of polystyrene, while the hydrogen production efficiency was similar. The yield of CO generation for Ni-WC/MgWO$_4$/MgAl$_2$O$_4$ reached the 27.6 ± 1.38 mmol/g$_p$ and for Ni-WC/Al$_2$O$_3$ 16.82 ± 0.84 mmol/g$_p$. The differences in carbon monoxide generation for catalysts mainly were the main factor affecting the H_2/CO ratio in the outlet stream. The methane contents in outlet streams also differed for particular plastics. It was observed that methane generation yields were similar for catalysed and uncatalyzed processes. The highest amounts were observed in the case od PCDR of low-density polyethylene.

The differences in the total amount of syngas obtained are the result of two factors: the type of feed fed into the reforming stage and the properties of the catalyst. The structure of the polymer determines the type of volatile compounds subjected to reforming in the second stage of the process. The complexity of the structures of these compounds determines whether the reforming reaction will result in complete conversion to hydrogen and carbon monoxide or whether intermediate products with a simpler structure will be produced, thereby reducing the efficiency of syngas generation. LDPE decomposes into short molecular compounds, which are easily reformed into CO and H_2. During pyrolysis, PS decomposes mainly into aromatic compounds (styrene and toluene),

Table 1

Syngas, liquid and solid residue yields for processes with and without the catalysts.

Plastic type	Parameter		No catalyst	Ni-WC/ MgWO$_4$/ MgAl$_2$O$_4$	Ni-WC/ Al$_2$O$_3$
LDPE	Syngas generation yield [mmol/g$_p$]	H_2	4.55 ± 0.33	18.01 ± 0.91	18.05 ± 0.39
		CO	5.45 ± 0.28	30.19 ± 1.51	25.44 ± 1.27
		CH$_4$	5.21 ± 0.25	5.87 ± 0.31	6.06 ± 0.31
		H_2 + CO	10.00 ± 0.51	48.20 ± 2.41	43.49 ± 2.17
	H_2/CO [-]		0.83	0.60	0.71
	Liquid yield [g/g$_p$]		0.17	0.09	0.15
	Solid residue/char [g/g$_p$]		0.01	0.01	0.02
PS	Syngas generation yield [mmol/g$_p$]	H_2	2.01 ± 0.11	8.93 ± 0.45	7.56 ± 0.38
		CO	3.58 ± 0.18	27.6 ± 1.38	16.82 ± 0.84
		CH$_4$	0.82 ± 0.04	0.73 ± 0.04	1.04 ± 0.05
		H_2 + CO	5.59 ± 0.28	36.53 ± 1.86	24.38 ± 1.21
	H_2/CO [-]		0.56	0.32	0.45
	Liquid yield [g/g$_p$]		0.46	0.49	0.44
	Solid residue/char [g/g$_p$]		0.01	0.01	0.02
PET	Syngas generation yield [mmol/g$_p$]	H_2	0.85 ± 0.05	6.42 ± 0.32	7.43 ± 0.37
		CO	2.32 ± 0.12	19.57 ± 0.98	19.13 ± 0.95
		CH$_4$	1.05 ± 0.06	0.71 ± 0.04	0.91 ± 0.05
		H_2 + CO	3.17 ± 0.17	25.99 ± 1.21	25.56 ± 1.33
	H_2/CO [-]		0.37	0.33	0.39
	Liquid yield [g/g$_p$]		0.02	0.01	0.07
	Solid residue/char [g/g$_p$]		0.49	0.54	0.53
SWP	Syngas generation yield [mmol/g$_p$]	H_2	2.29 ± 0.12	12.57 ± 0.61	12.00 ± 0.58
		CO	12.78 ± 0.64	28.24 ± 1.45	17.55 ± 0.92
		CH$_4$	1.13 ± 0.06	2.73 ± 0.14	3.52 ± 0.19
		H_2 + CO	15.17 ± 0.78	40.81 ± 2.21	29.55 ± 1.37
	H_2/CO [-]		0.19	0.45	0.68
	Liquid yield [g/g$_p$]		0.19	0.03	0.6
	Solid residue/char [g/g$_p$]		0.06	0.06	0.07

which, when applied to the catalyst bed, are reformed into simpler compounds. However, these compounds are in the liquid state under normal conditions, which is why high values of the obtained liquid products were observed. TG/DTG results also showed that the type of plastic influences the deactivation due to coking and/or oxidation of the catalyst. The degree of deactivation is closely related to catalyst properties. Higher activities were obtained for each plastic material for the Ni-WC/MgWO$_4$/MgAl$_2$O$_4$ catalyst. Compared to Ni-WC/Al$_2$O$_3$, Ni-WC/MgWO$_4$/MgAl$_2$O$_4$ catalyst was characterized by a smaller crystallite size, higher basicity, lower content of unbound carbon after the synthesis stage, and stronger interactions between the active phase and the support, resulting in higher H_2-TPR peak values. Ni-WC/MgWO$_4$/MgAl$_2$O$_4$ catalysts were characterized by coking to a lesser extent than that of Ni-WC/Al$_2$O$_3$. XPS results of the spent catalysts revealed that the surface composition after the PCDR process was similar for both the

catalysts. Therefore, the differences in the degree of coking may be explained by the differences in basicity. The basic characteristics of Ni-WC/MgWO$_4$/MgAl$_2$O$_4$ promote the gasification of the carbon deposits. It can also be noted that in the case of Ni-WC/Al$_2$O$_3$, coking occurs mainly during the PCDR process, which is visible mainly in the TG/DTG and XRD results; in the case of Ni-WC/MgWO$_4$/MgAl$_2$O$_4$, coking occurs to a lesser extent but to a greater extent in the formation of MgWO$_4$, which can also be catalytically active and enhance interactions between Ni-W elements.

4. Conclusions

In summary, Ni-WC/MgWO$_4$/MgAl$_2$O$_4$ and Ni-WC/Al$_2$O$_3$ catalysts were synthesized using a hydrothermal method followed by carbothermal reduction at 980 °C and passivation. The renewable saccharide glucose was used as a carbon source. The activity and stability of the catalysts were tested in pyrolysis combined with dry reforming (PCDR) of three types of plastics: low-density polyethylene (LDPE), polystyrene (PS), polyethylene terephthalate (PET), and their mixture (SWP). The process comprises two steps: pyrolysis of the plastic feedstock and dry reforming of the formed pyrolytic gases. The PCDR processes were conducted in the presence and absence of catalysts.

The PCDR process allows for resource recovery from waste. During the process gas and liquid fuels are generated. Syngas production for processes with catalysts was several times higher for each of the tested plastics than for processes without a catalyst. This proves the measurable benefits of using the catalyst in the recovery of raw materials via the PCDR route. For example, for the PCDR low-density polyethylene carried out with Ni-WC/MgWO$_4$/MgAl$_2$O$_4$ catalyst, the total value of syngas generated was 48.20 ± 2.41 mmol/g$_p$, while for uncatalyzed process equaled 10.00 ± 0.51 mmol/g$_p$. It was found that the properties of the plastics strongly determined the efficiency of gas, liquid, and solid product distribution, as well as the structural changes in the catalyst. The efficiency of gas fraction generation was in the following order: LDPE>PS>PET. The highest amounts of the liquid fraction were observed for PS, whereas the highest values of solid residue were observed for PET. Owing to the differences in the distribution of the obtained solid, liquid, and gaseous products, it is possible to control the composition of the output streams by selecting the appropriate catalyst and plastic feed.

The differences in the properties of the individual plastics affected the structural changes in the Ni-WC/MgWO$_4$/MgAl$_2$O$_4$ and Ni-WC/Al$_2$O$_3$ spent catalysts.

- In the case of the PCDR of polystyrene, preservation of the carbide crystal structure was observed for both catalysts. However, the formation of amorphous carbon deposits was identified based on the TG/DTG profiles.
- In the case of the PCDR of PET using the Ni-WC/MgWO$_4$/MgAl$_2$O$_4$ catalyst, oxidation to MgWO$_4$ and W$_3$O$_8$ was observed. In the case of Ni-WC/Al$_2$O$_3$, despite oxidation to tungsten oxide, the formation of graphitic carbon was identified. For the Ni-WC/MgWO$_4$/MgAl$_2$O$_4$ catalyst, the XRD peaks assigned to C overlapped with those of the MgWO$_4$ phase. For both the catalysts, the mass loss observed during the TG test was the smallest, indicating the highest degree of oxidation of the samples.
- After the PCDR of the LDPE and SWP spent catalysts were characterized by the largest mass loss observed in the TG profiles. The position of the DTG peaks for this polymer was at the highest temperature, which indicates the formation of carbon with an ordered structure of graphitic carbon [88].

Despite the influence of the plastic type on the decomposition of the products, differences in activity were observed between the two catalysts. The most significant differences were observed in the amount of generated carbon monoxide. For each PCDR process, higher summary amounts of syngas were observed for the Ni-WC/MgWO$_4$/MgAl$_2$O$_4$. The Ni-WC/MgWO$_4$/MgAl$_2$O$_4$ catalyst was characterized with smaller crystallite sizes for both phases of nickel and tungsten carbide, stronger interactions between the active phase and the support and higher basicity compared to Ni-WC/Al$_2$O$_3$. Higher basicity of the Ni-WC/MgWO$_4$/MgAl$_2$O$_4$ catalyst promoted carbon deposits gasification. Formation of MgWO$_4$ phase may also improve the Ni-WC/MgWO$_4$/MgAl$_2$O$_4$ activity. These properties are crucial for reforming of pyrolysis volatiles and carbon dioxide activation and the further reaction to hydrogen and carbon monoxide.

The obtained results indicate the high potential of carbide catalysts for the PCDR process, and may be a starting point for further research on the development of carbide catalytic materials for effective pyrolysis combined with dry reforming.

CRediT authorship contribution statement

Conceptualization; Izabela Wysocka. Methodology; Izabela Wysocka, Barbara Kościelska, Adam Kubiak. Validation; Izabela Wysocka, Barbara Kościelska, Jacek Gębicki. Formal analysis; Izabela Wysocka, Barbara Kościelska, Jacek Gębicki, Michał Maciejewski, Jakub Karczewski, Andrzej Rogala. Investigation; Izabela Wysocka, Barbara Kościelska, Jacek Gębicki, Michał Maciejewski, Jakub Karczewski, Andrzej Rogala. Resources; Izabela Wysocka, Adam Kubiak. Data Curation; Izabela Wysocka. Writing - Original Draft; Izabela Wysocka, Andrzej Rogala. Writing - Review & Editing; Izabela Wysocka, Jacek Gębicki, Andrzej Rogala. Visualization; Izabela Wysocka, Michał Maciejewski. Supervision; Izabela Wysocka, Jacek Gębicki. Project administration; Izabela Wysocka. Funding acquisition; Izabela Wysocka.

Declaration of Competing Interest

The authors declare that they have no known competing financial interests or personal relationships that could have appeared to influence the work reported in this paper.

Data Availability

Data will be made available on request.

Appendix A. Supporting information

Supplementary data associated with this article can be found in the online version at doi:10.1016/j.jece.2023.111298.

References

[1] W. Leal Filho, A.L. Salvia, A. Minhas, A. Paço, C. Dias-Ferreira, The COVID-19 pandemic and single-use plastic waste in households: a preliminary study, Sci. Total Environ. 793 (2021), 148571, https://doi.org/10.1016/j.scitotenv.2021.148571.

[2] N. Parashar, S. Hait, Plastics in the time of COVID-19 pandemic: protector or polluter? Sci. Total Environ. 759 (2021), 144274 https://doi.org/10.1016/j.scitotenv.2020.144274.

[3] J. Soffietti, A. Devard, F. Miranda, F. Akhter, F. Marchesini, Catalytic approaches for the removal of microplastics from water: recent advances and future opportunities, Chem. Eng. J. Adv. 16 (2023), 100529, https://doi.org/10.1016/j.ceja.2023.100529.

[4] E. Yousif, R. Haddad, Photodegradation and photostabilization of polymers, especially polystyrene: review, Springerplus 2 (398) (2013) 1–32, https://doi.org/10.1186/2193-1801-2-398.

[5] S. Huang, H. Wang, W. Ahmad, A. Ahmad, N.I. Vatin, A.M. Mohamed, A.F. Deifalla, I. Mehmood, Plastic waste management strategies and their environmental aspects: a scientometric analysis and comprehensive review, Int. J. Environ. Res. Public Health 19 (8) (2022), https://doi.org/10.3390/ijerph19084556.

[6] N. Evode, S.A. Qamar, M. Bilal, D. Barceló, H.M.N. Iqbal, Plastic waste and its management strategies for environmental sustainability, Case Stud. Chem. Environ. Eng. 4 (September) (2021), https://doi.org/10.1016/j.cscee.2021.100142.

[7] M. Ilyas, W. Ahmad, H. Khan, S. Yousaf, K. Khan, S. Nazir, Plastic waste as a significant threat to environment - a systematic literature review, Rev. Environ. Health 33 (4) (2018) 383–406, https://doi.org/10.1515/reveh-2017-0035.

[8] Y. Wang, Y. Li, L. Yang, X. Fan, L. Chu, Ca12Al14O33 or MgO supported Ni-carbide slag Bi-functional materials for H2 production and CO2 capture in sorption-enhanced steam gasification of cellulose/polyethylene mixture, Fuel 328 (April) (2022), 125209, https://doi.org/10.1016/j.fuel.2022.125209.

[9] L. Deng, W. Guo, H. Hao, X. Zhang, D. Wei, Q. Wei, Novel catalysts in catalytic upcycling of common polymer wastes, Chem. Eng. J. 471 (2023), 144350, https://doi.org/10.1016/j.cej.2023.144350.

[10] N.M. Hesam, J.M. Saad, A.H. Shamsuddin, M.F.M.A. Zamri, A.A. Rahman, A. F. Ghazali, Pyrolysis kinetic study of homogenized waste plastic and date blend, IOP Conf. Ser. Earth Environ. Sci. 476 (1) (2020), https://doi.org/10.1088/1755-1315/476/1/012135.

[11] A. Ochoa, J. Bilbao, A.G. Gayubo, P. Castaño, Coke formation and deactivation during catalytic reforming of biomass and waste pyrolysis products: a review, Renew. Sustain. Energy Rev. 119 (February 2019) (2020), https://doi.org/10.1016/j.rser.2019.109600.

[12] P. Singh, N. Déparrois, S. Burra, S. Bhattacharya, A.K. Gupta, Energy recovery from cross-linked polyethylene wastes using pyrolysis and CO2 assisted gasification, Appl. Energy 254 (February) (2019), 113722, https://doi.org/10.1016/j.apenergy.2019.113722.

[13] D. Saebea, P. Ruengrit, A. Arpornwichanop, Y. Patcharavorachot, Gasification of plastic waste for synthesis gas production, Energy Rep. 6 (2020) 202–207, https://doi.org/10.1016/j.egyr.2019.08.043.

[14] C. Wu, P.T. Williams, Pyrolysis-gasification of plastics, mixed plastics and real-world plastic waste with and without Ni-Mg-Al catalyst, Fuel 89 (10) (2010) 3022–3032, https://doi.org/10.1016/j.fuel.2010.05.032.

[15] S.S. Sharma, V.S. Batra, Production of hydrogen and carbon nanotubes via catalytic thermo-chemical conversion of plastic waste: review, J. Chem. Technol. Biotechnol. 95 (1) (2020) 11–19, https://doi.org/10.1002/jctb.6193.

[16] S. Kumagai, T. Yoshioka, Chemical feedstock recovery from hard-to-recycle plastics through pyrolysis-based approaches and pyrolysis-gas chromatography, Bull. Chem. Soc. Jpn. 94 (10) (2021) 2370–2380, https://doi.org/10.1246/bcsj.20210219.

[17] M. Olazar, L. Santamaria, G. Lopez, E. Fernandez, M. Cortazar, A. Arregi, J. Bilbao, Progress on catalyst development for the steam reforming of biomass and waste plastics pyrolysis volatiles: a review, Energy Fuels 35 (21) (2021) 17051–17084, https://doi.org/10.1021/acs.energyfuels.1c01666.

[18] J.M. Saad, P.T. Williams, Pyrolysis-catalytic dry (CO2) reforming of waste plastics for syngas production: influence of process parameters, Fuel 193 (2017) 7–14, https://doi.org/10.1016/j.fuel.2016.12.014.

[19] I. Aminu, M.A. Nahil, P.T. Williams, Pyrolysis-plasma/catalytic reforming of post-consumer waste plastics for hydrogen production, Catal. Today 420 (2023), 114084, https://doi.org/10.1016/j.cattod.2023.114084.

[20] J.M. Saad, P.T. Williams, Manipulating the H2/CO ratio from dry reforming of simulated mixed waste plastics by the addition of steam, Fuel Process. Technol. 156 (2017) 331–338, https://doi.org/10.1016/j.fuproc.2016.09.016.

[21] M. Al-asadi, N. Miskolczi, Hydrogen rich products from waste HDPE/LDPE/PP/PET over Me/Ni-ZSM-5 catalysts combined with dolomite, J. Energy Inst. 96 (2021) 251–259, https://doi.org/10.1016/j.joei.2021.03.004.

[22] J.M. Saad, P.T. Williams, Pyrolysis-catalytic-dry reforming of waste plastics and mixed waste plastics for syngas production, Energy Fuels 30 (4) (2016) 3198–3204, https://doi.org/10.1021/acs.energyfuels.5b02508.

[23] I. Barbarias, G. Lopez, M. Artetxe, A. Arregi, L. Santamaria, J. Bilbao, M. Olazar, Pyrolysis and in-line catalytic steam reforming of polystyrene through a two-step reaction system, J. Anal. Appl. Pyrolysis 122 (2016) 502–510, https://doi.org/10.1016/j.jaap.2016.10.006.

[24] E. Pawelczyk, I. Wysocka, J. Gębicki, Pyrolysis combined with the dry reforming of waste plastics as a potential method for resource recovery — a review of process parameters and catalysts, Catalysts 12 (4) (2022) 362.

[25] X. Gao, Z. Ge, G. Zhu, Z. Wang, J. Ashok, S. Kawi, Reforming of methane: recent progress and prospects, Catalysts 11 (2021) 1–19.

[26] N.A.K. Aramouni, J.G. Touma, B.A. Tarboush, J. Zeaiter, M.N. Ahmad, Catalyst design for dry reforming of methane: analysis review, Renew. Sustain. Energy Rev. 82 (June 2017) (2018) 2570–2585, https://doi.org/10.1016/j.rser.2017.09.076.

[27] A.G.S. Hussien, K. Polychronopoulou, A review on the different aspects and challenges of the dry reforming of methane (DRM) reaction, Nanomaterials 12 (19) (2022), https://doi.org/10.3390/nano12193400.

[28] M. Al-Asadi, N. Miskolczi, High temperature pyrolysis of municipal plastic waste using Me/Ni/ZSM-5 catalysts: the effect of metal/nickel ratio, Energies 13 (5) (2020), https://doi.org/10.3390/en13051284.

[29] J. Deng, L. Meng, D. Ma, Y. Zhou, X. Wang, X. Luo, S. Yuan, High H2 selective performance of Ni-Fe-Ca/H-Al catalysts for steam reforming of biomass and plastic, J. Energy Chem. 80 (2023) 215–227, https://doi.org/10.1016/j.jechem.2023.02.001.

[30] Q.L.M. Ha, H. Atia, C. Kreyenschulte, H. Lund, S. Bartling, G. Lisak, S. Wohlrab, U. Armbruster, Effects of modifier (Gd, Sc, La) addition on the stability of low Ni

[31] Q.L.M. Ha, H. Lund, C. Kreyenschulte, S. Bartling, H. Atia, T.H. Vuong, S. Wohlrab, U. Armbruster, Development of highly stable low Ni content catalyst for dry reforming of CH4-rich feedstocks, ChemCatChem 12 (6) (2020) 1562–1568, https://doi.org/10.1002/cctc.201902066.

[32] K. Akubo, M.A. Nahil, P.T. Williams, Co-pyrolysis–catalytic steam reforming of cellulose/lignin with polyethylene/polystyrene for the production of hydrogen, Waste Dispos. Sustain. Energy 2 (3) (2020) 177–191, https://doi.org/10.1007/s42768-020-00047-8.

[33] N. Czaplicka, A. Rogala, I. Wysocka, Metal (Mo, W, Ti) carbide catalysts: synthesis and application as alternative catalysts for dry reforming of hydrocarbons—a review, Int. J. Mol. Sci. 22 (22) (2021), https://doi.org/10.3390/ijms222212337.

[34] J.M. Saad, M.A. Nahil, C. Wu, P.T. Williams, Influence of nickel-based catalysts on syngas production from carbon dioxide reforming of waste high density polyethylene, Fuel Process. Technol. 138 (2015) 156–163, https://doi.org/10.1016/j.fuproc.2015.05.020.

[35] A.S. Al-Fatesh, N.Y.A. AL-Garadi, A.I. Osman, F.S. Al-Mubaddel, A.A. Ibrahim, W. U. Khan, Y.M. Alanazi, M.M. Alrashed, O.Y. Alothman, From plastic waste pyrolysis to fuel: impact of process parameters and material selection on hydrogen production, Fuel 344 (February) (2023), 128107, https://doi.org/10.1016/j.fuel.2023.128107.

[36] Y. Chai, N. Gao, M. Wang, C. Wu, H2 production from Co-pyrolysis/gasification of waste plastics and biomass under novel catalyst Ni-CaO-C, Chem. Eng. J. 382 (2020) 122947, https://doi.org/10.1016/j.cej.2019.122947.

[37] H. Yamada, H. Mori, T. Tagawa, CO2 reforming of waste plastics, J. Ind. Eng. Chem. 16 (1) (2010) 7–9, https://doi.org/10.1016/j.jiec.2010.01.029.

[38] Y. Jin, D. Liu, X. Li, R. Yang, Synthesis of WC nanopowders from novel precursors, Int. J. Refract. Met. Hard Mater. 29 (3) (2011) 372–375, https://doi.org/10.1016/j.ijrmhm.2011.01.007.

[39] R. Li, A. Shahbazi, L. Wang, B. Zhang, C.C. Chung, D. Dayton, Q. Yan, Nanostructured molybdenum carbide on biochar for CO2 reforming of CH4, Fuel 225 (2018) 403–410, https://doi.org/10.1016/j.fuel.2018.03.179.

[40] C. Wang, H. Lei, X. Kong, R. Zou, M. Qian, Y. Zhao, W. Mateo, Catalytic upcycling of waste plastics over nanocellulose derived biochar catalyst for the coupling harvest of hydrogen and liquid fuels, Sci. Total Environ. 779 (2021), 146463, https://doi.org/10.1016/j.scitotenv.2021.146463.

[41] X. Zhang, J. Wang, G. Zhang, J. Liu, Y. Wang, Y. Zhao, G. Li, Co–Ni/WC-AC catalysts for dry reforming of methane: the role of Ni species, Int. J. Hydrog. Energy 48 (40) (2023) 15065–15076, https://doi.org/10.1016/j.ijhydene.2022.12.360.

[42] Q. Zhang, L. Pastor-Pérez, S. Gu, T.R. Reina, Transition Metal Carbides (TMCS) Catalysts For Gas Phase CO2 upgrading reactions: a comprehensive overview, Catalysts 10 (9) (2020), https://doi.org/10.3390/catal10090955.

[43] Z. Lin, S.R. Denny, J.G. Chen, Transition metal carbides and nitrides as catalysts for thermochemical reactions, J. Catal. 404 (2021) 929–942, https://doi.org/10.1016/j.jcat.2021.06.022.

[44] C. Shi, A. Zhang, X. Li, S. Zhang, A. Zhu, Y. Ma, C. Au, Ni-Modified Mo 2C catalysts for methane dry reforming, 431–432, Appl. Catal. A Gen. (2012) 164–170, https://doi.org/10.1016/j.apcata.2012.04.035.

[45] C.B. Rodella, D.H. Barrett, S.F. Moya, S.J.A. Figueroa, M.T.B. Pimenta, A.A. S. Curvelo, V. Teixeira Da Silva, Physical and chemical studies of tungsten carbide catalysts: effects of Ni promotion and sulphonated carbon, RSC Adv. 5 (30) (2015) 23874–23885, https://doi.org/10.1039/c5ra03252k.

[46] U. Kanerva, M. Karhu, J. Lagerbom, A. Kronlöf, M. Honkanen, E. Turunen, T. Laitinen, Chemical synthesis of WC-Co from water-soluble precursors: the effect of carbon and cobalt additions to WC synthesis, Int. J. Refract. Met. Hard Mater. 56 (2016) 69–75, https://doi.org/10.1016/j.ijrmhm.2015.11.014.

[47] S. Li, G. Zhang, J. Wang, J. Liu, Y. Lv, Enhanced activity of Co catalysts supported on tungsten carbide-activated carbon for CO2 reforming of CH4 to produce syngas, Int. J. Hydrog. Energy 46 (56) (2021) 28613–28625, https://doi.org/10.1016/j.ijhydene.2021.06.085.

[48] I. Wysocka, N. Czaplicka, E. Pawelczyk, J. Karczewski, J. Sobczak, Z. Bielan, M. Maciejewski, B. Kościelska, A. Rogala, Novel sugar-based nickel-tungsten carbide catalysts for dry reforming of hydrocarbons, J. Ind. Eng. Chem. 124 (2023) 431–446, https://doi.org/10.1016/j.jiec.2023.04.038.

[49] A.D. Lalsare, B. Leonard, B. Robinson, A.C. Sivri, R. Vukmanovich, C. Dumitrescu, W. Rogers, J. Hu, Self-regenerable carbon nanofiber supported Fe – Mo2C catalyst for CH4-CO2 assisted reforming of biomass to hydrogen rich syngas, Appl. Catal. B Environ. 282 (2021), 119537, https://doi.org/10.1016/j.apcatb.2020.119537.

[50] C.H. Kim, Y.G. Hur, K.Y. Lee, Relationship between surface characteristics and catalytic properties of unsupported Nickel-Tungsten carbide catalysts for the hydrocracking of vacuum residue, Fuel 309 (2022), 122103, https://doi.org/10.1016/j.fuel.2021.122103.

[51] L. Fu, W. Xia, MAX phases as nanolaminate materials: chemical composition, microstructure, synthesis, properties, and applications, Adv. Eng. Mater. 23 (4) (2021) 1–31, https://doi.org/10.1002/adem.202001191.

[52] M. Sherif El-Eskandarany, M. Omori, T.J. Konno, K. Sumiyama, T. Hirai, K. Suzuki, Synthesizing of nanocomposite WC/MgO powders by mechanical solid-state reduction and subsequent plasma-activated sintering, Metall. Mater. Trans. A Phys. Metall. Mater. Sci. 32 (1) (2001) 157–164, https://doi.org/10.1007/s11661-001-0111-0.

[53] A. Hajalilou, M. Hashim, R. Ebrahimi-Kahizsangi, I. Ismail, N. Sarami, Synthesis of titanium carbide and TiC-SiO2 nanocomposite powder using rutile and Si by mechanically activated sintering, Adv. Powder Technol. 25 (3) (2014) 1094–1102, https://doi.org/10.1016/j.apt.2014.02.008.

[54] L. Yao, Y. Wang, M.E. Galvez, C. Hu, P. Da Costa, Ni–Mo2C supported on alumina as a substitute for Ni–Mo reduced catalysts supported on alumina material for dry reforming of methane, Comptes Rendus Chim. 21 (3–4) (2018) 247–252, https://doi.org/10.1016/j.crci.2017.06.002.

[55] M. Abou Hamdan, A. Nassereddine, R. Checa, M. Jahjah, C. Pinel, L. Piccolo, N. Perret, Supported molybdenum carbide and nitride catalysts for carbon dioxide hydrogenation, Front. Chem. 8 (452) (2020) 1–12, https://doi.org/10.3389/fchem.2020.00452.

[56] M. Lewandowski, R. Janus, M. Wadrzyk, A. Szymańska-Kolasa, C. Sayag, G. Djéga-Mariadassou, On catalytic behavior of bulk Mo2c in the hydrodenitrogenation of indole over a wide range of conversion thereof, Catalysts 10 (11) (2020) 1–14, https://doi.org/10.3390/catal10111355.

[57] A.F. Lamic, T.L.H. Pham, C. Potvin, J.M. Manoli, G. Djéga-Mariadassou, Kinetics of bifunctional isomerization over carbides (Mo, W), J. Mol. Catal. A Chem. 237 (1–2) (2005) 109–114, https://doi.org/10.1016/j.molcata.2005.03.041.

[58] A.J. Brungs, A.P.E. York, J.B. Claridge, C. Márquez-Alvarez, M.L.H. Green, Dry reforming of methane to synthesis gas over supported molybdenum carbide catalysts, Catal. Lett. 70 (3–4) (2000) 117–122, https://doi.org/10.1023/A:1018829116093.

[59] L. Jia, C. Li, Y. Zhao, B. Liu, S. Cao, D. Mou, T. Han, G. Chen, Y. Lin, Interfacial engineering of Mo2C-Mo3C2 heterononowires for high performance hydrogen evolution reactions, Nanoscale 11 (48) (2019) 23318–23329, https://doi.org/10.1039/c9nr08986a.

[60] Q. Gao, C. Zhang, S. Xie, W. Hua, Y. Zhang, N. Ren, H. Xu, Y. Tang, Synthesis of nanoporous molybdenum carbide nanowires based on organic - inorganic hybrid nanocomposites with sub-nanometer periodic structures, Chem. Mater. 21 (23) (2009) 5560–5562, https://doi.org/10.1021/cm9014578.

[61] H. Lin, B. Tao, J. Xiong, Q. Li, Y. Li, Tungsten Carbide (WC) nanopowders synthesized via novel core-shell structured precursors, Ceram. Int. 39 (3) (2013) 2877–2881, https://doi.org/10.1016/j.ceramint.2012.09.061.

[62] M. Islam, R. Martinez-Duarte, A sustainable approach for tungsten carbide synthesis using renewable biopolymers, Ceram. Int. 43 (13) (2017) 10546–10553, https://doi.org/10.1016/j.ceramint.2017.05.118.

[63] K.F. Wang, S.Q. Jiao, K.C. Chou, G.H. Zhang, A facile pathway to prepare ultrafine WC powder via a carbothermic pre-reduction followed by carbonization with CH4-H2 mixed gases, Int. J. Refract. Met. Hard Mater. 86 (September 2019) (2020), 105118, https://doi.org/10.1016/j.ijrmhm.2019.105118.

[64] R.A. Mir, O.P. Pandey, Waste plastic derived carbon supported Mo2C composite catalysts for hydrogen production and energy storage applications, J. Clean. Prod. 218 (2019) 644–655, https://doi.org/10.1016/j.jclepro.2019.02.004.

[65] I. Wysocka, A. Mielewczyk-Gryń, M. Łapiński, B. Cieślik, A. Rogala, Effect of small quantities of potassium promoter and steam on the catalytic properties of nickel catalysts in dry/combined methane reforming, Int. J. Hydrog. Energy 46 (5) (2021) 3847–3864, https://doi.org/10.1016/j.ijhydene.2020.10.189.

[66] K.S.W. Sing, D.H. Everett, R.A.W. Haul, L. Moscou, A. P. R, J. Rouquerol, T. Siemieniewska, Reporting physisorption data for gas/solid systems with special reference to the determination of surface area and porosity, J. Polym. Sci. Part A Polym. Chem. 57 (4) (1985) 603–619, https://doi.org/10.1002/pola.26338.

[67] P. Bretzler, M. Huber, S. Nickl, K. Köhler, Hydrogenation of furfural by noble metal-free nickel modified tungsten carbide catalysts, RSC Adv. 10 (46) (2020) 27323–27330, https://doi.org/10.1039/d0ra02003f.

[68] Y. Jin, D. Liu, X. Li, R. Yang, Synthesis of WC nanopowders from novel precursors, Int. J. Refract. Met. Hard Mater. 29 (3) (2011) 372–375, https://doi.org/10.1016/j.ijrmhm.2011.01.007.

[69] P.D. Bhuyan, D. Singh, S. Kansara, P. Yadav, S.K. Gupta, Y. Sonvane, S.K. Rout, E. Sinha, Experimental and theoretical analysis of electronic and optical properties of MgWO4, J. Mater. Sci. 52 (9) (2017) 4934–4943, https://doi.org/10.1007/s10853-016-0730-x.

[70] S. Li, J. Wang, G. Zhang, J. Liu, Y. Lv, Y. Zhang, Highly stable activity of cobalt based catalysts with tungsten carbide-activated carbon support for dry reforming of methane, Fuel 311 (October 2021) (2022), 122512, https://doi.org/10.1016/j.fuel.2021.122512.

[71] G. Singla, K. Singh, O.P. Pandey, Synthesis of carbon coated tungsten carbide nano powder using hexane as carbon source and its structural, thermal and

[72] electrocatalytic properties, Int. J. Hydrog. Energy 40 (16) (2015) 5628–5637, https://doi.org/10.1016/j.ijhydene.2015.02.127.

[72] C. Falco, N. Baccile, M.M. Titirici, Morphological and structural differences between glucose, cellulose and lignocellulosic biomass derived hydrothermal carbons, Green. Chem. 13 (11) (2011) 3273–3281, https://doi.org/10.1039/c1gc15742f.

[73] E. García-Bordejé, E. Pires, J.M. Fraile, Parametric study of the hydrothermal carbonization of cellulose and effect of acidic conditions, Carbon N. Y 123 (2017) 421–432, https://doi.org/10.1016/j.carbon.2017.07.085.

[74] D. Jung, M. Zimmermann, A. Kruse, Hydrothermal carbonization of fructose: growth mechanism and kinetic model, ACS Sustain. Chem. Eng. 6 (11) (2018) 13877–13887, https://doi.org/10.1021/acssuschemeng.8b02118.

[75] M.I. Zaki, N.E. Fouad, S.A.A. Mansour, A.I. Muftah, Temperature-programmed and X-ray diffractometry studies of hydrogen-reduction course and products of WO3 powder: influence of reduction parameters, Thermochim. Acta 523 (1–2) (2011) 90–96, https://doi.org/10.1016/j.tca.2011.05.004.

[76] P.V. Krasovskii, O.S. Malinovskaya, A.V. Samokhin, Y.V. Blagoveshchenskiy, V.A. Kazakov, A.A. Ashmarin, XPS Study of Surface Chemistry of Tungsten Carbides Nanoproduced through DC Thermal Plasma/Hydrogen Annealing Process, Appl. Surf. Sci. 339 (1) (2015) 46–54, https://doi.org/10.1016/j.apsusc.2015.02.152.

[77] I. Mazo, L.E. Vanzetti, J.M. Molina-Aldareguia, A. Molinari, V.M. Sglavo, Role of surface carbon nanolayer on the activation of flash sintering in tungsten carbide, Int. J. Refract. Met. Hard Mater. 111 (December 2022) (2023), 106090, https://doi.org/10.1016/j.ijrmhm.2022.106090.

[78] G. Leclercq, M. Kamal, J.M. Giraudon, P. Devassine, L. Feigenbaum, L. Leclercq, A. Frennet, J.M. Bastin, A. Löfberg, S. Decker, et al., Study of the preparation of bulk powder tungsten carbides by temperature programmed reaction with CH4 + H2 Mixtures, J. Catal. 158 (1) (1996) 142–169, https://doi.org/10.1006/jcat.1996.0015.

[79] A. Younis, J. Estephane, C. Gennequin, L. Tidahy, B. El Khoury, S. Aouad, E. Abi Aad, Influence of promoting Ni-based catalysts with ruthenium in the dry reforming of polypropylene plastics for syngas production, Int. J. Hydrog. Energy 7 (2022), https://doi.org/10.1016/j.ijhydene.2022.07.156.

[80] D.K. Binte Mohamed, A. Veksha, Q.L.M. Ha, W.P. Chan, T.T. Lim, G. Lisak, Advanced Ni tar reforming catalysts resistant to syngas impurities: current knowledge, research gaps and future prospects, Fuel 318 (2022), 123602, https://doi.org/10.1016/j.fuel.2022.123602.

[81] X. Chen, X. Ma, X. Peng, Role of filamentous coke in deactivation of Ni/Bio-char catalyst during dry reforming of non-oxygenates tar, J. Anal. Appl. Pyrolysis 159 (381) (2021), 105314, https://doi.org/10.1016/j.jaap.2021.105314.

[82] I. Wysocka, B. Kościelska, M. Maciejewski, E. Pawelczyk, TG and DTG profiles for plastics: LDPE, HDPE, PP, PD and PET [Data Set], Gdan. Univ. Technol.: Gdan. (2023).

[83] T.P. Wampler, Thermometric behavior of polyolefins, J. Anal. Appl. Pyrolysis 15 (1989) 187–195, https://doi.org/10.1016/0165-2370(89)85032-6.

[84] M. Day, D. Wiles, Influence of temperature and environment on the thermal decomposition of poly(ethylene terephthalate) fibres with and without the flame retardant tris(2,3-dibromopropyl)phosphate, J. Anal. Appl. Pyrolysis 7 (1984) 65–82.

[85] J.M. Encinar, J.F. González, Pyrolysis of synthetic polymers and plastic wastes. Kinetic study, Fuel Process. Technol. 89 (7) (2008) 678–686, https://doi.org/10.1016/j.fuproc.2007.12.011.

[86] J. Alvarez, S. Kumagai, C. Wu, T. Yoshioka, J. Bilbao, M. Olazar, P.T. Williams, Hydrogen production from biomass and plastic mixtures by pyrolysis-gasification, Int. J. Hydrog. Energy 39 (21) (2014) 10883–10891, https://doi.org/10.1016/j.ijhydene.2014.04.189.

[87] D.K. Ojha, R. Vinu, Resource recovery via catalytic fast pyrolysis of polystyrene using zeolites, J. Anal. Appl. Pyrolysis 113 (2015) 349–359, https://doi.org/10.1016/j.jaap.2015.02.024.

[88] J.M. Saad, P.T. Williams, Catalytic dry reforming of waste plastics from different waste treatment plants for production of synthesis gases, Waste Manag. 2016 (58) (2016) 214–220, https://doi.org/10.1016/j.wasman.2016.09.011.